

## **Response**

We thank the referees for their additional comments, which are addressed below.

Furthermore, after taking a close look at the paper with the modification made, we made some additional changes to the discussion (section 4) for the part between lines 684 and 711. Parts of this section were moved to either section 3.1 or the discussion section, and the remainder of the part between lines 684 and 711 has been adjusted for readability and consistency.

**Referee #1**

We have included/modified the suggested technical corrections.

## Referee #2

- We modified the discussion and conclusions so that it should be clear now where the “30-60%” originates from (table 7) and how to interpret those numbers.
- We rephrased the last sentence of the Abstract, explaining what we mean when we talk about “choices”:

“... uncertainties in parameters and independent variables and choices in defining the optimal time period and area for calculating the ozone record and the independent variables ...”

Note that it is important to realize that both uncertainties in parameters and choices in time period and area over which to average hamper detection of recovery.

- We modified the discussion, giving less prominence to the notion that for some certain regressors extending the period does not always lead to higher significance. This discussion was originally added to show that all uncertainties discussed in the paper leave (quite) some room for interpretation and that not all results conform to prior expectations. It is therefore tempting to focus only on favorable results confirming prior expectations while neglecting unfavorable results, so we wanted to make sure that the unfavorable results (although minor) are mentioned.
- We added a sentence noting that Solomon et al. [2005] show that there appear to be some volcanic effects in height resolved ozone during the ozone hole season, but that these effects are too small in magnitude and vertical extend to leave a detectable impact in total ozone. When looking superficially there still appears to be some change in total ozone related to volcanic activity, but Poberaj [2011] show that these are more likely related to (coincidental) dynamical effects than to volcanic aerosols. Our study as well as those of Knibbe et al. [2014] confirm the lack of volcanic signal in total ozone. We made sure that in the discussion our results only apply to total ozone, not height resolved ozone.
- Adding the finding that we do find positive post-break trends in ozone (1.66 to 4.74 DU/year; 95% CI) is an important finding. It is one of the requirements for detection of ozone recovery, and despite uncertainties with regard to trend significance ALL trends in ozone are positive. There was no a priori reason to assume that had to be the case, and it is consistent with various other studies noting that although trends may not necessarily be statistically significant, they tend to be positive. No changes made.
- See also second comment. We added the explanation in the Abstract of what hampers detection (uncertainties in data AND choices for area and time period over which to average). That way the Abstract and Conclusions are consistent.
- Line 767-769: deleted the sentence. It is now implicitly included in the previous section.
- Added a sentence to both the discussion and conclusions section about the relation between statistical significance and length of the record noting that our results suggest that with continued extension of the total ozone record and using multi-variate regressions detection of Antarctic ozone hole recovery may be reached before 2020.

This is what our findings imply (see table 7). Currently (2010 or 2012) we are around 50% statistical significance. Our results also indicate that for each year added the significance increases by approximately 10 % (order of magnitude). Although just a ball-park estimate, it suggests that by 2020 you may expect to have passed the 95% confidence level.

- Caption changed. Table 5 shows the results for the time series ending in 2010 for all break years (97, 98, 99). Also adjusted the description of table 5 in the discussion section.

### Referee #3

#### General comment & discussion on trend error calculation

Thanks to the extensive response of referee #3 we now finally understand where the differences stem from with regard to the trend error calculations in Kuttippurath et al. [2013] and ours. In essence there are different aspects relevant for the trend errors.

- (A) The EESC regression parameter (C5 in referee #3 comment) has an associated error
- (B) Linear regression of EESC multiplied with regression parameter (C5) pre-break and post-break have their own associated errors
- (C) Residual of the multi-variate regression

In Kuttippurath et al. [2013] equations (2) and (3) of the #R3 report are used for calculating pre-break and post-break ozone trends. Equations (4) and (5) of the #R3 report are used to calculate the pre-break and post-break ozone trend errors.

In particular, the ozone trend error is calculated as:

$$\frac{dO_3}{dt} \underset{\substack{\text{error} \\ \text{time period}}}{=} = EESC_{\text{error}} \times \frac{dEESC}{dt} \underset{\text{time period}}{}$$

For trend error calculations the pre-break and post-break linear trends in the EESC must be calculated. These linear trends have their own errors because of the fact that the shape of the pre-break and post-break EESC curve are not completely linear.

In our paper we calculate trend errors based solely on this last step, which results in fairly small trend errors.

If we calculate the trend error based on the method in Kuttippurath et al. [2013] we find order of magnitude similar values similar to those of Kuttippurath et al. [2013], and indeed the post-break trend error is proportional to pre-break trend error via the ratio of the pre-break and post-break trends in EESC. See table values in bold.

Both methods describe two different error sources and should be taken into account together. For the case discussed here the error associated with the EESC regression dominates the error from the linear regression on both pre-break and post-break trends. See table values in bold + italics

Period	Kuttippurath et al. [2013]		This study	
	EESC	PWLT	EESC	PWLT
1979-1999	-4.50 ± 0.65	-5.02 ± 1.11	-5.39 ± 0.22 <b>-5.39 ± 0.97</b> <b><i>-5.39 ± 0.99</i></b>	-5.66 ± 1.03
2000-2010	1.11 ± 0.16	2.91 ± 2.73	1.04 ± 0.12 <b>1.04 ± 0.19</b> <b><i>1.04 ± 0.22</i></b>	3.30 ± 2.85

However, after further consideration of the method applied in Kuttippurath et al. [2013] we argue that the method applied there is mathematically not justified and leads to conceptual problems. Underlying reason is that the error associated with the EESC regression is only valid for the entire EESC time series, not parts of it, as outlined below.

Consider the following hypothetical situation with the following EESC shape: the pre-break increase is as the current EESC but the post-break changes is flat (zero). According to equation (5) of the #R3 report and the equation here above, the associated ozone trend error would then be zero regardless of the regression parameter (C5).

This is counter-intuitive: in case of similar noise levels, one would expect that the smaller the trend, the larger the trend error. Or at least a non-zero trend error.

The EESC regression error applies to the entire record and should be considered as such. Because of the particular shape of the EESC (increase-decrease) the regression error will be largely determined by corresponding long term changes in ozone (decrease-increase), not the year-to-year changes in ozone. However, for the two separate periods one would expect the trend errors to also be dependent on the year-to-year variations in ozone (the sign change in EESC which dominates the fit with the total ozone record does not matter anymore in case of the two separate periods). Hence, the post-regression separation in two periods should be considered very carefully.

This is highlighted by the very different trend errors of the PWLT fit (see table above). Whereas the EESC-associated error is considerably smaller for the post-BREAK period compared to the pre-BREAK period, the PWLT trend errors show exactly the opposite: the pre-BREAK trend error is much smaller than the post-break trend error. The latter is more intuitive: the pre-BREAK period is longer and the trend is larger, which should result in smaller trend errors.

In summary, we argue that we think the calculation of trend uncertainty in Kuttippurath et al. [2013] is not justified, and that as far as we are concerned it is unclear how to actually do that (other than *a posteriori* applying a sort of piece-wise linear trend calculation, which then should be included in the regression to start with rather than be applied *a posteriori*). Trend errors as derived from the method applied in Kuttippurath et al. [2013] are counter intuitive: one would expect larger trend errors for the post-BREAK period, not smaller. The PWLT errors do are consistent with this notion. If the goal is to determine pre-break and post-break trends and errors, then the fit parameter should consist of two separate parts, as is done when including the PWLT in the regression.

We have modified sections 3.1 and the discussion in section 4, as well as table 3 according to the discussion above. Note that we have not referred to this in the in the abstract or the conclusions, as that would put too much emphasis on it and there were already sufficient arguments to argue that use of EESC in the regression is not preferred.

## Specific comments

Line 28: included

Line 34-35, changed to “the onset of recovery of the Antarctic Ozone Hole”

Line 70-71, changed to “Both studies do not consider the effect of deterministic variations in ozone on estimating when the onset and complete recovery of the Antarctic ozone hole recovery occur.”

Line 202-203. This is a tricky point. Salby et al. [2012] indeed only identify 2002 as an outlier. However, Weber et al [2003, 2011] and updates in the upcoming WMO 2014 ozone assessment report indicate that in both hemispheres there are outlier years that ‘skew’ the statistics.

We suggest to modify the text and make it more specific and use somewhat less strong wording.

“The Arctic and Antarctic may behave very similar [Weber et al., 2003; 2011] or much less similar [Salby et al., 2012]. This is because the notion of hemispheric similarities in how the EP flux affects ozone depletion so far may be biased by a few outlier years (2002 and 2006 for the SH, 1996, 2010 and 2011 for the NH).”

Line 515-517. Section between lines 511-517 was completely changed.

“Note that there is slight difference in the 1979-1999 trends for the period ending in 2010 and 2012 because of the difference in total record length, which results in slightly different regression coefficients. However, calculating trend errors for the EESC-based pre-BREAK and post-BREAK trends in ozone using the EESC regression error as done in Kuttippurath et al. (2013) is not justified. The trend errors depend on the actual trend values themselves (see table 3): the EESC-fit based post-break trend error is much smaller than the pre-BREAK trend. In the hypothetical case of no (zero) trend the trend error would also be zero, which would be physically unrealistic. The PWLT on the other hand shows opposite differences in trend errors: the post-BREAK trend error is much larger than the pre-BREAK trend error, conform expectations.”

Line 560-562. Correct, should be table 3. We did an additional check on all table and references to them in the paper as there had been a change in table numbering between versions.

Line 563-565. See discussion above about trend errors.

Line 626. Figure 3 should be figure 4 (middle panel). The lower panel of figure 6 also shows a tri-modal distribution. Text adjusted accordingly.

Line 638. Text adjusted accordingly.

Line 652. Text adjusted accordingly.

Line 653-654. See discussion above about different approaches on trend error calculations. Answer: the EESC fit uncertainty will be largely determined by the long term changes in ozone (decrease-increase), not the year-to-year variations. However, when separating the decreasing and increasing part of the EESC,

the year-to-year variations should be considered as the sign change in long term ozone changes do not matter anymore.

Line 707-711. Reading the comment, we think that the referee actually refers to the previous section (696-706). This section was replaced by the next statement, which is less pessimistic and does more justice to our analysis. It shows that there is a balance: a gain in confidence by removing some deterministic variations in ozone, but with some adverse effects as the multi-variate regression introduces new uncertainties. The section then ends on a positive note (lines 707-711):

“Furthermore, this implies that with continued extension of the total ozone record detection of Antarctic ozone recovery may be reached before 2020 using multi-variate regressions. Note that although in total the number of statistically significant trends increases with record length, this is not necessarily always the case (compare Table 5 and Table 6 – thus BREAK-2010 vs. 1998-2012 trends).

On the other hand, the trend significance level if significant trends is generally between  $2\sigma$  and  $3\sigma$  (not shown), indicating that a considerable amount of variability is not accounted for in the regression. Our analysis also shows that detection of the 2<sup>nd</sup> stage of ozone recovery based on just one arbitrary selected (set of) regressor – ozone record combination(s) does not reflect the structural uncertainties present in the underlying data.

Nevertheless, the appearance of larger groups of statistically significant results occurring for longer time series and a certain persistence among ozone scenarios and EP flux scenarios shows that these type of analyses are capable of removing deterministic variations in average ozone, and that with increasing length of the post-break period more statistically significant results can be expected.”

Line 724-727: see discussion above. Now that we fully understand what was done in Kuttippurath et al. (2013) we argue that that method does not take the fit residuals into account.

Line 735. The larger range of trends in the PWLT compared to the EESC fits is indicative of the limited use of the EESC – its post-peak trend is largely determined by the pre-defined EESC shape and thus does not do justice to all uncertainties. This is what we refer to as a lack of flexibility when using the EESC to determine post-BREAK ozone trends.

Line 774. Suggestion to change to “are expected”, rather than “may” or “will”, because we expect that future updates of this analysis provide better clues about the onset of recovery.

Table 5. Table caption modified (ending 2010).

Line 977. Typical maximum wind speed numbers added (20-30 m/s)

Line 982. Typo corrected.

Line 1000-1026.

Figures 6-7. Suggestion included.



1 Tracing the second stage of Antarctic ozone hole recovery with a “big data”

2 | approach to **multi-multivariate** regressions

3

4 A.T.J. de Laat, R.J. van der A, M. van Weele

5

6 Royal Netherlands Meteorological Institute, De Bilt, The Netherlands.

7

8

9 **Abstract**

10

11 | This study presents a sensitivity analysis of ~~multi~~-multivariate regressions of recent  
12 | springtime Antarctic vortex ozone trends using a “big data” ensemble approach.

13 | Our results indicate that the poleward heat flux (Eliassen-Palm Flux) and the effective  
14 | chlorine loading explain, respectively, most of the short-term and long-term variability in  
15 | different Antarctic springtime total ozone records. The inclusion in the regression of  
16 | stratospheric volcanic aerosols, solar variability and the Quasi-Biennial Oscillation is  
17 | shown to increase rather than to decrease the overall uncertainty in the attribution of  
18 | Antarctic springtime ozone because of large uncertainties in their respective records.

19 | Calculating the trend significance for the ozone record from the late 1990s onwards  
20 | solely based on the fit of the effective chlorine loading is not recommended, as this does  
21 | not take fit residuals into account resulting in too narrow uncertainty intervals, while the  
22 | fixed temporal change of the effective chlorine loading does not allow for any flexibility  
23 | in the trends.

24 | When taking fit residuals into account into a piecewise linear trend fit, we find that  
25 | approximately 30-60% of the regressions in the full ensemble result in a statistically  
26 | significant positive springtime ozone trend over Antarctica from the late 1990s  
27 | ~~onwards~~to 2010 or 2012. Analysis of choices and uncertainties in time series show that,  
28 | depending on choices in time series and parameters, the fraction of statistically significant  
29 | trends in parts of the ensemble can range from negligible to a complete 100%. We also  
30 | find that, consistent with expectations, the number of statistically significant trends  
31 | increases with increasing record length.

32 | Although our results indicate that the use ~~multi-multi~~variate regressions is a valid  
33 | approach for assessing the state of Antarctic ozone hole recovery, and it can be expected  
34 | with increasing record length results will move towards more confidence in recovery,  
35 | uncertainties in parameters and independent variables and choices in ~~uncertainties in~~  
36 | ~~choices~~ defining the optimal time period and area for calculating the ozone record and the  
37 | independent variables currently do not yet support formal identification of the onset of  
38 | recovery of the Antarctic Ozone Hole.  
39

40 **1. Introduction**

41

42 An important question in 21<sup>st</sup> century ozone research is whether the ozone layer is  
43 starting to recover as a result of the measures taken to reduce emissions of Ozone  
44 Depleting Substances (ODS) as agreed on in the Montreal Protocol [UNEP, 2012] and its  
45 subsequent amendments and adjustments.

46 The World Meteorological Organization has defined three different stages of ozone  
47 recovery [WMO, 2007]. The first stage consists of a slowing of ozone depletion,  
48 identified as the occurrence of a statistically significant reduction in the rate of decline in  
49 ozone due to changing stratospheric halogens. The second stage revolves around the  
50 onset of ozone increase (turnaround), identified as *the occurrence of statistically*  
51 *significant increases in ozone - above a previous minimum value - that can be attributed*  
52 *to declining stratospheric halogens*. Note that what is meant by “statistically significant”  
53 is not specified. Finally, the third stage is the full recovery of ozone from ODSs,  
54 identified as when the ozone layer is no longer affected by ODSs, or alternatively, once  
55 stratospheric ozone levels have returned to pre-1980 values.

56 The first stage of ozone recovery has already been identified in observations to have  
57 occurred roughly in the late 1990s [WMO 2007, 2011]. The third stage is not expected to  
58 occur until somewhere halfway the 21<sup>st</sup> century or later [WMO, 2011]. The spatial  
59 distribution of total ozone after the third stage probably differs somewhat from the pre-  
60 1980 distribution due to climate change – in particular changes in the stratospheric  
61 chemical composition and temperature structure [Bekki et al., 2011, and references  
62 therein].

63 As far as the second stage of ozone recovery is concerned, it has recently been argued  
64 that a statistically significant increase in ozone beyond a minimum and attributable to  
65 decreases in ODSs can be identified for the Antarctic ozone hole [Salby et al., 2011,  
66 2012; Kuttippurath et al., 2013; Knibbe et al., 2014]. To some extent this is surprising as it  
67 has long been thought that identification of the second stage of ozone recovery could only  
68 be expected after 2020 [e.g. Newman et al., 2006; Eyring et al., 2007]. Those estimates  
69 were based on (model) simulations of ozone from which it is calculated when the ozone  
70 trend from a certain starting year onwards would qualify for “statistically significant”, or  
71 in other words, would emerge from the year-to-year natural variations in ozone (“noise”).

72 ~~Such methods implicitly assume Both studies do not consider the effect of deterministic~~  
73 ~~variations in ozone on estimating when the onset and complete recovery of the Antarctic~~  
74 ~~ozone hole recovery occur. that ozone variations around the trend are not deterministic~~  
75 ~~(random).~~

76 However, it has also long been established that many stratospheric ozone variations are  
77 in fact deterministic. Various processes have been identified that affect stratospheric  
78 ozone variability in the Southern Hemisphere on an ~~inter-annual~~interannual basis, like  
79 volcanic aerosols [Telford et al., 2009], the Southern Annular Mode (SAM) [Thompson  
80 and Wallace, 2000; Jiang et al., 2008], the poleward heat flux or Eliassen-Palm flux (EP  
81 flux) [Randel et al., 2002], solar variability [Soukharev and Hood, 2006], and the Quasi  
82 Biennial Oscillation (QBO) [Jiang et al., 2008]. If the physics and chemistry are  
83 sufficiently understood, it might be possible to filter out part of the ozone variations from  
84 the ozone records by means of a multi-variatey regression, resulting in a smoother ozone  
85 record for which trend significance might be reached earlier. This approach, in essence,

86 forms the basis of the suggested identification of the second stage of ozone recovery  
87 reported by Salby et al. [2011, 2012], Kuttippurath et al. [2013] and Knibbe et al [2014].

88 However, none of these studies did systematically consider the uncertainties in the  
89 proxies that were selected for the regressions. In addition, no motivation or discussion  
90 was provided for the choice of a specific ozone record, *e.g.* a consideration of taking  
91 annual, seasonal, and/or monthly means of total ozone, and the integration over a chosen  
92 spatial domain.

93 Hence, we want to address the following question in this study: Is the suggested  
94 detection of the second stage of ozone recovery robust when uncertainties in the  
95 regression parameters and for different selected ozone records are taken into account?  
96 This question is approached here with combined multiple scenario – Monte Carlo  
97 ensemble simulations using the same regression methodology as presented in  
98 Kuttippurath et al. [2013] but by inclusion of various uncertainties leading to a large  
99 ensemble of different regressions. We analyze this “big data” ensemble for robustness of  
100 the individual regressions.

101 Kuttippurath et al. [2013] considered different Antarctic vortex definitions and thus  
102 different vortex ozone records. They found that regression results were not very sensitive  
103 to the Antarctic vortex definition. Hence, we decided to use September-November  
104 Antarctic vortex core (poleward of 70°S) average total ozone column based on the Multi  
105 Sensor Reanalysis (MSR; van der A et al. [2010]), also because from a practical point of  
106 view this definition does not require additional information about the location of the  
107 vortex edge. The selected regressors are the SAM, solar flux, QBO, EP flux, stratospheric  
108 volcanic aerosols and the Equivalent Effective Stratospheric Chlorine (EESC), similar to

109 Kuttippurath et al. [2013]. The EESC can be used to estimate ozone trends. Kuttippurath  
110 et al. [2013] also calculated Piece Wise Linear Trends (PWLT) for estimating ozone  
111 trends as alternative for the EESC-based ozone trends, an approach we will follow here as  
112 well.

113 In this paper, we extend the analysis by introducing both several differing scenarios for  
114 the ozone record and regressor records of the EP flux, volcanic aerosols, and EESC.  
115 Monte Carlo variations were applied to the regressor records of the solar flux, QBO,  
116 SAM by adding random variations. While we focus on parameter uncertainties in this  
117 study, additional uncertainties do exist, for example with respect to possible time lags  
118 between regressors and the ozone record. The resulting ensemble of regression results  
119 provides a big data pool of about 23 million different regressions that is analyzed in terms  
120 of probability distributions of the explanatory power of the regressions ( $R^2$ ), the ozone  
121 trends and corresponding ozone trend uncertainties, and the regression coefficient values  
122 quantifying the dependence of ozone on a particular regressor. We also investigate if  
123 some way of optimization is possible for the chosen scenarios, and we discuss the  
124 likelihood of detection of the second stage of ozone recovery within the context of all  
125 uncertainties presented. Note that the uncertainties discussed here differ from formal  
126 errors that come with a standard ~~multi~~-multivariate regression. Also note that we  
127 implicitly assume that the relation between the independent variables and ozone is linear,  
128 even though the relation may very well be non-linear. The latter will to some extent be  
129 considered in our study and is part of the discussion of the results, but the issue of non-  
130 linearity of the regressor-ozone relation is not addressed in detail, in particular because,

131 as will be shown, for many regressors the non-linearity of its relation with ozone is  
132 insufficiently characterized, or even unknown.

133 This paper is organized as follows. Section 2 describes the observational datasets used  
134 and the ozone and regressor scenarios or Monte Carlo simulations performed. Section 3  
135 discusses the probability distributions of the explanatory power of the regressions, trends  
136 and regression values, including how the distributions depend on scenarios or Monte  
137 Carlo results. Section 4 discusses the question of detection of the second stage of ozone  
138 recovery, and in section 5 everything is wrapped up and some conclusions are drawn.

139

## 140 **2. Multivariate regression parameter uncertainties**

141

142 Online data sources of the ozone observation records and applied regressors can be  
143 found in Table 1.

144

### 145 **2.1 Method**

146

147 A common method for analyzing total ozone records is the use of a ~~multi-~~multivariate  
148 linear regression, a method that we will use in this paper as well. The goal of the method  
149 is to attribute both ~~inter-annual~~interannual as well as decadal variations in the ozone  
150 record to processes that are expected or known to affect the total ozone record  
151 (Kuttippurath et al. [2013], and references therein). In the regression, the total ozone  
152 variability (Y) as a function of time (t) is expressed as

153



$$\begin{aligned}
154 \quad & Y(t) = K && \text{(Constant)} \\
155 \quad & + C_1 HF(t) && \text{(Poleward Heat Flux or Eliassen-Palm (EP) flux)} \\
156 \quad & + C_2 SAM(t) && \text{(Southern Annual Mode index)} \\
157 \quad & + C_3 (SF \times QBO)(t) && \text{(Solar Flux} \times \text{QBO index)} \\
158 \quad & + C_4 Aer(t) && \text{(Stratospheric Aerosol optical depth)} \\
159 \quad & + C_5 Trend(t) && \text{(Total ozone trend)} \\
160 \quad & + \varepsilon(t) && \text{(Total ozone residual)}
\end{aligned}$$

161

162 In which  $t$  is the time from 1979 to 2010 or 2012,  $K$  is a constant and regression  
163 coefficients  $C_1$  to  $C_5$  are the regression coefficients for the respective proxies. The ozone  
164 trend ( $C_5$ ) can be related to the time-dependent equivalent effective stratospheric chlorine  
165 loading (EESC) or a piecewise linear trend (PWLT) before and after a predefined break  
166 year. The PWLT regressions are calculated by including two linear terms in the  
167 regression: the first term is a linear fit for the entire time window, the second term is a  
168 linear term only for the years after a chosen break year [Kuttippurath et al., 2013].

169 The analysis of regression results will focus on two parameters that have previously  
170 been used in papers investigating Antarctic ozone recovery [Yang et al., 2008; Salby et  
171 al., 2011, 2012; Kuttippurath et al., 2013; Knibbe et al., 2014]: the serial correlation  $R$   
172 between the regression-based ‘reconstructed’ ozone record and the observations, and the  
173 post-break trends and trend significance. Since the focus of our paper is to investigate  
174 trend significance, not specifically what parameters can best explain Antarctic ozone, we  
175 will only look in some detail at the usefulness of certain regressors. However, our  
176 analysis does provide indications of what are more and less useful regressors.

177 In sections 2.2 to 2.7 the uncertainty in each of the proxies that is used as a regressor is  
178 discussed. These uncertainty ranges determine the spread in the ensemble that is used in  
179 the “big data” analysis. A summary of the regressor uncertainties and how they are  
180 incorporated in this study can be found in Table 2. The solar flux and QBO are combined  
181 into one proxy as discussed in section 2.3.

182

## 183 **2.2 Poleward heat flux (EP flux)**

184

185 Figure 1 shows the poleward heat flux, here represented by the (vertical) EP flux  
186 [Andrews et al., 1987] at the 70-hPa level and averaged poleward of 40°S for the  
187 combined months of August and September, as well as the average EP flux available for  
188 a given year for a variety of datasets. Note that the datasets do not all completely overlap  
189 in time. Before 2000 there are considerable differences between the datasets. After 2000  
190 these differences are smaller, which to some extent is traced to the lack of ERA40 data  
191 beyond 2001 and lack of JRA data beyond 2004. The lower panel shows the relative  
192 differences between the five datasets and their mean. The standard deviation of all data is  
193 7.65%, but from 2000 onwards only 2.67%.

194 Another source of uncertainty in the use of the EP flux as proxy is the choice of the  
195 time window over which the average EP flux is calculated. This choice depends on what  
196 is thought to be the relationship between variations in EP flux and ozone depletion. The  
197 basic theory states that the poleward movement of stratospheric air is proportional to the  
198 strength of the residual mean stratospheric circulation (Brewer-Dobson circulation),  
199 which in turn is driven by the poleward eddy heat flux. The poleward eddy heat flux is

200 expressed by the upward component of the Eliassen-Palm flux that measures the upward  
201 transport of momentum by planetary waves [Andrews et al., 1987; Salby et al., 2012, and  
202 references therein]. Planetary wave activity in the Northern Hemisphere affects Arctic  
203 Polar vortex stability and thus Arctic ozone depletion. However, to what extent this is  
204 similar in the Southern Hemisphere is still a topic of debate. The Arctic and Antarctic  
205 may behave ~~either-very~~ similarly [Weber et al., 2003; 2011] or ~~not-much less similar~~  
206 [Salby et al., 2012]. This is because the notion of hemispheric similarities in how the EP  
207 flux affects ozone depletion so far ~~is-may be heavily-biased on-by only-one a few~~ outlier  
208 years (2002 ~~and 2006~~ for the SH, ~~-1996, 2010 and~~ 2011 for the NH).

209 Current research efforts try to gain a better understanding of the physical and  
210 photochemical mechanisms by which the heat flux and planetary wave action affects  
211 Antarctic stratospheric ozone. A recently proposed mechanism [de Laat and van Weele,  
212 2011] involves a pre-conditioning of Antarctic inner stratospheric vortex air whereby  
213 stratospheric temperatures affect PSC formation which in turn affects the buildup of a  
214 halogen reservoir that later during Austral spring changes the rate of catalytic ozone  
215 destruction. This preconditioning mechanism explains some years with anomalous ozone  
216 depletion, but not all. For example, during Austral winter 2013 the Antarctic vortex  
217 remained largely undisturbed – opposite to 2010 and 2012, see de Laat and van Weele  
218 [2011] and Klekociuck et al. [2011], thus allowing for widespread PSC formation and  
219 pre-conditioning the inner vortex air for efficient ozone depletion. However, from the  
220 start of Austral spring 2013 (halfway August) onwards the Antarctic stratospheric vortex  
221 got disturbed by planetary wave activity. As a result, the amount of springtime ozone  
222 depletion remained below what has been experienced during previous years with similar

223 preconditioning. This suggests that there are multiple pathways as well as complicated  
224 interactions between chemistry and physics that can lead to reduced Antarctic springtime  
225 ozone depletion. Hence, it is unclear which regressor or regressors could act as proxies  
226 for these complex processes.

227 A further complicating factor is the disintegration of the Antarctic vortex, which is  
228 again controlled by planetary wave activity [Kramarova et al., 2014]. The stability of the  
229 vortex determines how long the ozone depleted inner-vortex air remains intact after  
230 photochemical ozone depletion ceases during Austral spring. Variations in the duration of  
231 Antarctic vortex stability introduce variations in the Antarctic total ozone record which  
232 are not related to variations in photochemistry.

233 We attempt to reflect these issues in our uncertainty range for the proxy used to account  
234 for the EP flux variations in multivariate regressions. Salby et al. [2011, 2012] and  
235 Kuttippurath et al. [2013] use the August – September mean EP flux poleward of 40°S  
236 and at the 70-hPa level, the baseline also used in this study. Weber et al. [2011] uses the  
237 100-hPa poleward heat flux rather than the 70-hPa heat flux and the average over the  
238 region between 45°S and 75°S rather than between 40°S and 90°S. They further show that  
239 there is no particular favorable wintertime month or period from the perspective of  
240 Antarctic springtime ozone depletion over which to average the EP flux. Hence there is a  
241 certain arbitrariness involved in selecting the optimum EP flux averaging period and  
242 region.

243 For our study we define eight different EP flux scenarios, using different periods,  
244 latitudes and heights (see Table 2), all based on the ECMWF ERA Interim dataset.  
245 Performing the same exercise as in Figure 1 for these eight scenarios, the standard

246 deviation of the EP flux time series is 21.5%. This is considerably larger than the  
247 variability among the same EP fluxes of the different reanalysis datasets discussed above.  
248 Thus, the uncertainty in EP flux estimates largely originates in using different periods,  
249 latitudes and/or heights for which the EP flux is calculated, rather than in the use of  
250 different reanalysis datasets to calculate the same EP flux.

251

252

### 253 **2.3 The mixed solar-QBO index**

254

255 In Kuttippurath et al. [2013] the effects of solar variability and QBO variability are  
256 combined into one proxy. As explained in Holton and Tan [1990], in studying high-  
257 latitude variability and trends the QBO and solar effects cannot be considered separately.  
258 Whereas the solar influence modifies tropical stratospheric ozone and dynamics, the  
259 transport of the solar signal to higher/polar latitudes depends on the phase of the QBO.  
260 As a result, solar effects on winter polar Antarctic stratospheric temperatures also depend  
261 on the phase of the QBO [Labitzke, 2004]. If the QBO is westerly (easterly), stratospheric  
262 temperatures vary in phase (out of phase) with solar activity. It has been proposed by  
263 Haigh and Roscoe [2006] and Roscoe and Haigh [2007] to combine the QBO and solar  
264 activity into a new regression index that takes this effect into account:

$$265 \quad \text{Solar-QBO index} = (\text{Solar} - S_m) \times (\text{QBO} - Q_m)$$

266 In which  $S_m$  is the mean of the solar flux and  $Q_m$  the midpoint of the QBO range.  
267 However, as Roscoe and Haigh [2007] note, this new index is rather sensitive to the  
268 choice of  $S_m$  and  $Q_m$ , in particular as the index is by construction the product of two

269 anomaly fields, and thus sensitive to sign changes. In addition, the choice of  $S_m$  and  $Q_m$  is  
270 also arbitrary. Roscoe and Haigh [2007] solve this by selecting averages for which the  
271 best total ozone column regression results are obtained. However, the best regression  
272 results may not necessarily mean that the regressor is the best representation of the  
273 underlying physical mechanism, in particular as regression results also depend on other  
274 proxies and in principle there can be a cancellation of errors from different proxies in the  
275 regression. Thus, the sensitivity of the combined solar-QBO index on the calculation  
276 method of the anomalies must be further investigated.

277 Figure 2 shows the resulting solar flux – QBO index time series, given various  
278 assumptions in its calculation. Clearly there is a considerable variability in the index  
279 values. The lower plot shows that the variability for every single anomaly varies by  $\pm$   
280 200%. This is rather large compared to the estimated uncertainties in both individual  
281 solar flux and QBO proxies. Hence, using a combined solar flux – QBO proxy introduces  
282 a considerable amount of additional uncertainty. For the uncertainty range in our  
283 regressions we construct 100 Monte Carlo time series in which for each single solar-flux  
284 QBO index value random Gaussian noise is added with an amplitude of 200% of the  
285 index value.

286 Note that the uncertainties in the individual QBO and solar flux proxies are much  
287 smaller than the uncertainty in the combined solar flux – QBO index which is relevant for  
288 high-latitude trends (see supplementary information for a separate discussion of the solar  
289 flux and QBO index).

290

## 291 **2.4 Southern Annular Mode**

292

293 The Southern Annular Mode (SAM) is a widely used index that reflects the zonal  
294 symmetry of the tropospheric circulation in the Southern Hemisphere. The symmetry of  
295 the Southern Hemisphere circulation has long been identified as an important mode of  
296 variability of the Southern Hemisphere climate. A positive index is characterized by  
297 anomalously high surface pressure at mid-latitudes and anomalously low surface pressure  
298 at latitudes closer to Antarctica.

299 The SAM used in this study is derived from the National Oceanic and Atmospheric  
300 Administration (NOAA). It is based on Empirical Orthogonal Functions (EOF) applied to  
301 the monthly mean National Centers for Environmental Prediction and National Center for  
302 Atmospheric Research (NCEP/NCAR) reanalysis [Kalnay et al., 1996] 700-hPa height  
303 anomalies poleward of 20°S for the Southern Hemisphere, with the seasonal cycle being  
304 removed. The monthly SAM index is constructed by projecting the daily and monthly  
305 mean 700-hPa height anomalies onto the leading EOF mode. Both time series are  
306 normalized by the standard deviation of the monthly index (1979-2000 base time period).  
307 Since the leading pattern of SAM is obtained using the monthly mean height anomaly  
308 dataset, the index corresponding to each loading pattern becomes one when it is  
309 normalized by the standard deviation of the monthly index.

310 However, there is no unique SAM index due to the existence of different  
311 meteorological datasets and different methods to quantify the symmetry of the Southern  
312 Hemisphere circulation. Kuttippurath et al. [2013] use the AntArctic Oscillation (AAO)  
313 index, which is in fact a certain choice of SAM index. A study by Ho et al. [2012]  
314 provides a comprehensive analysis of eight different SAM indices. Their analysis shows

315 that the correlation ( $R^2$ ) between the indices varies between 0.45 and 0.96 for seasonal  
316 values and 0.73 and 0.96 for monthly values. This corresponds with random (Gaussian)  
317 variations between 20-100% (root-mean-square value). For most of the indices the  
318 correlation is better than 0.75. As a point of reference, adding random Gaussian noise of  
319 50% to a time series of a parameter and calculating its correlation with the original time  
320 series results to a correlation ( $R^2$ ) of almost 0.8.

321 For the uncertainty analysis we construct 100 Monte Carlo time series in which for each  
322 single SAM index value Gaussian noise is added with – to be on the conservative side -  
323 an amplitude of 100% of the index value.

324

## 325 **2.5 EESC loading**

326

327 Uncertainties in the estimates of the EESC loading originate from two factors: the mean  
328 age-of-air, which reflects how fast stratospheric halogen concentrations decline due to  
329 transport velocity of halogen poor tropospheric air from the tropical stratosphere to the  
330 polar stratosphere, and the so-called ‘fractional release’, the rate with which Ozone  
331 Depleting Substances (ODSs) release chlorine and bromine in the stratosphere. ODSs  
332 typically have not yet been dissociated when they enter the stratosphere at the tropical  
333 tropopause, and thus have fractional release values of zero. After transiting through the  
334 upper stratosphere, the ODSs in an air parcel get fully dissociated due to their exposure to  
335 energetic radiation and the fractional release values get close to 1.0 [Newman et al.,  
336 2007].



337 To complicate matters, the mean age-of-air in the stratosphere is not a constant but  
338 varies with latitude, height and season [Stiller et al., 2008]. On average, the age-of-air  
339 increases with height, *i.e.* it takes longer for tropospheric air to travel higher in the  
340 stratosphere, and the age-of-air also increases towards the poles because of the time it  
341 takes for air to travel from the tropical “source” region to higher latitudes. In the  
342 Antarctic vortex regions there is a strong seasonal dependence of the age-of-air due to the  
343 isolation of inner vortex air during Austral winter and spring, while upper stratospheric  
344 and mesospheric air slowly descends in the Antarctic vortex. The descending air is  
345 particularly “old” air and causes strong vertical gradients in the age-of air in the  
346 wintertime polar vortex. Stiller et al. [2008; their figure 7] show that the age-of-air almost  
347 triples going up from 15 km ( $\theta = 400$  K; age-of-air  $\sim 4$  years), to 20 km ( $\theta = 400$  K; age-  
348 of air  $\sim 7$  years), to 25 km ( $\theta = 600$  K; age-of-air  $\sim 9$  years), to finally 30 km ( $\theta = 750$  K;  
349 age-of-air  $\sim 11$  years). How to account for this variability in a regression is unclear, but it  
350 is unlikely that one age-of-air value can be attributed to the total ozone column.

351 Moreover, ozone variability in the Antarctic vortex is determined by different processes  
352 at different altitudes. Halogen related ozone depletion typically maximizes between 15-20  
353 km altitude ( $\sim 100$ -50 hPa, US Standard atmosphere 1976;  $\theta = 400$ -500 K), whereas the  
354 effect of vortex stability on ozone depletion is seen predominantly between 20-30 km  
355 altitude ( $\sim 50$ -10 hPa;  $\theta = 500$ -750 K) [de Laat and van Weele, 2011]. Thus, total ozone  
356 columns observations which are vertically integrated amounts of ozone are being affected  
357 by different processes at different altitudes.

358 The age-of-air may also not be constant over the time period over which ozone trends  
359 are determined. Due to a changing climate the stratospheric circulation may speed up

360 [e.g. Engel et al., 2009; Bunzel and Schmidt, 2013], causing a decrease in the age-of-air  
361 with increased warming, which obviously then depends on the exact warming. This  
362 introduces yet another uncertainty for the periods from 1979 to 2010 or 2012 that are  
363 considered in this study.

364 The age-of-air uncertainties do not manifest themselves as a random process, which  
365 would make it useful for applying a Monte Carlo method, but as a structural uncertainty,  
366 *i.e.* the entire EESC shape would change for different parameter settings. Such  
367 uncertainty could be captured by applying a parametric bootstrap rather than a Monte  
368 Carlo approach. However, such parametric approach would also not suffice because we  
369 use total column observations and we know that ozone at different altitudes would be  
370 affected by different parameter values.

371 A pragmatic approach with regard to the sensitivity of the regression to EESC values is  
372 testing the robustness of the regression results as a function of the assumed EESC time  
373 evolution. For the uncertainty analysis we assume three different EESC scenarios with an  
374 age-of-air of 2.5, 4 and 5.5 years and a half-width of, respectively, 1.25, 2 and 2.75 years.  
375 Largest differences between the three scenarios are in their post-peak trend in EESC (see  
376 later on in Figure 3).

377

## 378 **2.6 Volcanic aerosol.**

379

380 Aerosols from sufficiently strong volcanic eruptions can reach the stratosphere and  
381 affect stratospheric ozone chemistry. In particular strong eruptions occurring in the  
382 tropics can have long lasting effects on stratospheric ozone. Aerosols reaching the

383 tropical stratosphere are slowly transported towards middle and high latitudes. It can take  
384 up to a decade before the stratosphere is cleared from volcanic aerosols [Vernier et al.  
385 2011; Solomon et al., 2011]. Volcanic eruptions at middle and high latitudes have much  
386 shorter lasting effects. These aerosols enter in the descending branch of the stratospheric  
387 circulation and will be relatively quickly removed from the stratosphere.

388 The short-term effect of stratospheric volcanic aerosols is heating of the stratospheric  
389 layer which affects stratospheric ozone in the tropical belt. The dominant long-term effect  
390 of stratospheric volcanic aerosols on global and polar ozone is however the increase in  
391 aerosol surface area density and subsequent heterogeneous ozone loss. Model simulations  
392 of volcanic aerosol effects on stratospheric ozone suggest that in particular under cold  
393 conditions (high latitude, wintertime, lower stratosphere) total ozone columns can be  
394 reduced by up to 10-15 % [Rozanov et al., 2002]. During other seasons, total ozone  
395 column depletion by volcanic aerosols is of the order of a few percent.

396 Since 1979 two major tropical volcanic eruptions have affected stratospheric ozone: El  
397 Chichón, Mexico, in 1982, and Pinatubo, Philippines, in 1991. Although the total amount  
398 of stratospheric aerosols by both eruptions has been characterized relatively well, there  
399 appear to be considerable uncertainties associated with the time evolution of the aerosol  
400 amounts in the Southern Hemisphere. A brief and incomplete survey of a latitudinal  
401 volcanic aerosol radiative forcing data [Ammann et al., 2003] and a global volcanic  
402 aerosol proxy record [Crowley and Unterman, 2012] as well as the standard volcanic  
403 aerosol index used in Kuttippurath et al. [2013] – aerosol optical depth, Sato et al. [1993]  
404 and updates, available via NASA GISS – all show that there are large differences  
405 between the El Chichón aerosol peak relative to the Pinatubo peak. Large differences are

406 seen in global, hemispheric and Southern Hemisphere (Antarctic) aerosol amounts as  
407 well as differences in the exact timing of the peak aerosols [Sato et al., 1993; Ammann et  
408 al., 2003]; Crowley and Unterman, 2012]. The El Chichón aerosol peak relative to the  
409 Pinatubo peak for high Antarctic latitudes can be similar [Ammann et al., 2003], about  
410 three times smaller [Sato et al., 1993] to (globally) eight times smaller [Crowley and  
411 Unterman, 2012]. The Pinatubo peak aerosol in the Southern Hemisphere was about half  
412 the size of the global-mean Pinatubo peak [Ammann et al., 2003].

413 Kuttippurath et al. [2013] shift the Southern Hemisphere aerosol data by six months to  
414 account for the transport of aerosols. Although they report that the six month shift results  
415 in the best statistics, the analysis presented in the previous paragraph shows that the effect  
416 of the shift is relevant for the shape of the volcanic aerosol changes, but does not  
417 introduce variations as large as the other variations in volcanic aerosol indices. Given that  
418 a time shift is included in the 6 volcanic aerosol scenarios defined above, we do not add  
419 additional time shifts in the aerosol record.

420 We define six volcanic aerosol scenarios that reflect the uncertainty in the volcanic  
421 stratospheric aerosol records. Base scenario is the scenario used in Kuttippurath et al.  
422 [2013] which in turn uses the NASA GISS stratospheric aerosol record. A second  
423 scenario is with the Pinatubo aerosol curve scaled so that the maximum matches the El  
424 Chichón aerosol peak, the Pinatubo curve maximum is 2.5 times the El Chichón peak,  
425 and the Pinatubo curve maximum is five times the El Chichón peak. The uncertainty in  
426 timing of the Southern Hemispheric aerosol peak is considered by a shift of the El  
427 Chichón peak one year back compared to the Pinatubo peak and a shift of the Pinatubo  
428 peak one year back compared to El Chichón peak.

429

## 430 **2.7 Ozone Scenarios.**

431

432 It is *a priori* unclear what would be the most appropriate ozone scenario to use in the  
433 regression. Both Salby et al. [2011, 2012] and Kuttippurath et al. [2013] use the  
434 September-November three-month averaged total ozone record. However, as discussed in  
435 the introduction, different processes affect ozone during different time periods. Studies in  
436 the literature use very different time periods for averaging ozone to investigate Antarctic  
437 ozone trends. We define eight different ozone scenarios to reflect the ozone records used  
438 in literature (see also de Laat and van Weele [2011]), using the MSR dataset [van der A  
439 et al., 2010]. The MSR is a 30-year total O<sub>3</sub> column assimilation dataset for 1979–2008  
440 based on a total of eleven satellite instruments measuring total O<sub>3</sub> columns – including  
441 | SCIAMACHY - that were operating during various periods within these 30 years. For the  
442 | period 2009-2012 the MSR dataset was extended with assimilated SCIAMACHY and  
443 GOME-2 total ozone column data. Apart from the September-November three-month  
444 averaged total ozone record we also use averages of total ozone over the month of  
445 September, the month of October, the two-month period September-October, a very long  
446 period (19 July – 1 December), a very short 10-day period (21 – 30 September), the  
447 period 7 September – 13 October, and a year-dependent “worst” 30-day period (30-day  
448 average with the largest Ozone Mass Deficit).

449

## 450 **2.8 Other uncertainties**

451

452 Kuttippurath et al. [2013] address two other important uncertainties for the  
453 determination of the ozone trend. First, the area over which the ozone record is defined  
454 (Inside Vortex, Equivalent Latitude 65°S-90°S, and Vortex Core). The area is important  
455 for the absolute amounts of ozone depletion but Kuttippurath et al. [2013] show it is  
456 much less relevant for the differences in trend. That is, the uncertainties in the estimated  
457 linear trend dominate the uncertainties due to different areas over which the ozone  
458 anomalies are calculated. A second uncertainty on their ozone trend derives from the use  
459 of different ozone datasets (ground-based, TOMS/OMI and MSR). Also here the  
460 uncertainties in the estimated linear trend dominate the uncertainties due to the different  
461 data sets. Hence, we do not include these uncertainties in our analysis.

462 In addition, there are many studies trying to identify the moment where ODSs stop  
463 increasing and/or where ozone stops decreasing. The maximum ODSs appears  
464 somewhere between 1997 and 2000 (Newman et al., 2007), depending on geographical  
465 location and height. However, due to saturation effects – there are more than sufficient  
466 ODS present to destroy all Antarctic ozone – the moment where ozone starts to be  
467 affected by decreasing ODSs may actually be later (Kuttippurath et al., 2013; Kramarova  
468 et al., 2014).

469 The moment of a structural break in ozone based on observations indicates an early  
470 break around 1997 (Newchurch et al., 2003; Yang et al., 2008). However, some processes  
471 affecting stratospheric ozone vary on long time scales – solar effects and volcanic  
472 eruptions come to mind – which may affect the observations-based analysis of break  
473 points (Dameris et al., 2006). Note that we confirm this break year of 1997 based on a  
474 applying a break-point analysis algorithm to the MSR ozone record (not shown). Hence,

475 we decided to use three different break years that have been identified and/or are most  
476 commonly used: 1997, 1998 and 1999.

477

## 478 **2.9 Selected uncertainties ranges and ozone record scenarios.**

479

480 Figure 3 shows the baseline regressor time series and the scenarios for ozone, the EP flux,  
481 EESC loading and volcanic aerosols. A total of 100 different solar flux – QBO index and  
482 SAM index time series are used to span their uncertainty range (not shown in Figure 3).  
483 All scenarios and Monte Carlo results combined provide 11.5 million different choices  
484 for the regressions ( $100 \times 100 \times 8 \times 8 \times 6 \times 3$ ; see Table 2). Ozone trends are calculated based  
485 on the EESC loading or using a piecewise linear trend (PWLT) analysis. For the PWLT  
486 ensembles the three different EESC scenarios are irrelevant. Instead, the sensitivity of the  
487 regressions is tested using three different break years (1997, 1998 and 1999). In total we  
488 | analyze approximately 23 million ~~000~~-different trends using the EESC and PWLT  
489 scenarios.

490 Note that by basing our analysis on both different ozone and EP flux scenarios certain  
491 time-lag relations are taken into account. It should also be noted that the use of such a  
492 wide range of scenarios indicates that much remains unclear about what best describes  
493 Antarctic ozone depletion and the time-lag relations between ozone and explanatory  
494 variables.

495

## 496 **3 Scenario analysis**

497

### 498 3.1 Reproducing Kuttippurath et al., [2013].

499

500 First a ~~multi-multi~~variate regression is performed similar to Kuttippurath et al. [2013]  
501 in which the MSR dataset is used within the Vortex core (70°-90°S). The results are  
502 summarized in their Figure 5 and Table 4 which are duplicated here in Table 3 along with  
503 the results from a ~~multi-multi~~variate regression based on the same variables as used in  
504 Kuttippurath et al. [2013].

505 Our results reproduce the results from Kuttippurath et al. [2013], although there are  
506 minor differences in the absolute numbers, most likely related to differences in EP fluxes  
507 [Jayanarayanan Kuttippurath, *personal communication*, September 2013]. The trends for  
508 the periods 1979-1999 and for 2000-2010 are of comparable magnitude in both studies,  
509 as well as the PWLT significance levels for the period 1979-1999 and the EESC trends  
510 for both 1979-1999 and 2000-2010. The magnitude of the recovery for 2000-2010 based  
511 on the PWLT is slightly larger, but also in our analysis the post 2010 linear trend in  
512 ozone is significant beyond  $2\sigma$ . For the correlation of the regression model with the ozone  
513 record we obtain a value of 0.87 ( $R^2$ ) comparable to the 0.90 ( $R^2$ ) reported in  
514 Kuttippurath et al., [2013]. Thus, the results are sufficiently similar to proceed with  
515 studying the effects of the uncertainties in regressors and ozone record scenarios on the  
516 regression results. Note that there is slight difference in the 1979-1999 trends for the  
517 period ending in 2010 and 2012 because of the difference in total record length, which  
518 results in slightly different regression coefficients. ~~Note that we calculate the pre-break~~  
519 ~~and post-break EESC-based trends by applying linear regressions to the EESC curve~~  
520 ~~multiplied with the EESC regression coefficient for the pre-break and post-break time~~



521 ~~periods. As a result, EESC based trend errors are related to the non-linearity of the EESC~~  
522 ~~curve, and the trend errors differ for both the pre-break and post-break time periods. Our~~  
523 ~~EESC based trend errors differ from those in Kuttippurath et al (2013), which lacks a~~  
524 ~~description of how EESC based trend errors are calculated.~~

525 However, calculating trend errors for the EESC-based pre-BREAK and post-BREAK  
526 trends in ozone using the EESC regression error as done in Kuttippurath et al. (2013) is  
527 not justified. The trend errors depend on the actual trend values themselves (Table 3): the  
528 EESC-fit based post-break trend error is much smaller than the pre-BREAK trend. In the  
529 hypothetical case of no (zero) trend the trend error would also be zero, which would be  
530 physically unrealistic. The PWLT on the other hand shows hand shows opposite  
531 differences in trend errors: the post-BREAK trend error is much larger than the pre-  
532 BREAK trend error, conform expectations.

533

### 534 **3.2 Ozone record and regressor correlations.**

535

536 Before analyzing the ensemble of regression results it is important to investigate the  
537 correlations between the different regressors. If correlations between regressors are too  
538 large, they cannot be considered to be independent, and it should be decided which one to  
539 omit from the analysis, as the regression otherwise cannot separate which variability is  
540 related to which regressor. Furthermore, it is *a priori* useful to understand how regressors  
541 correlate with the ozone record, as a small correlation implies that a regressor can only  
542 explain a limited amount of ozone variability.

543 Table 4 shows the mean correlation between the different regressors and their  $2\sigma$  spread  
544 based on the ozone record and regressor selections and/or Monte Carlo results (SAM,  
545 SF×QBO index). The EP flux correlates positively with the EESC and negatively with  
546 the SAM and, to a lesser extent, also with the SF×QBO index. The other regressors do  
547 not show significant cross-correlations. Only for a few individual ozone record scenarios,  
548 regressor selections and Monte Carlo results cross-correlations are found to exceed 0.5.

549 The uncertainty in the correlations with the ozone records ranges between about 10%  
550 and 20% for each of the regressors. Small cross-correlations between the regressors  
551 however do not provide a justification for *a priori* omitting one of the regressors.

552

### 553 3.3 Trends.

554

555 Figure 4 shows the probability distributions of the ozone trends for 1979- $Y_B$  and  $Y_B$ -  
556 2012 periods, in which  $Y_B$  is the break year which can either be 1997, 1998 or 1999. For  
557 the 1979- $Y_B$  period the mean EESC trend is -5.56 DU/year (-4.00 to -7.06; 95% CI) and  
558 the mean PWLT trend is -6.40 DU/year (-4.22 to -7.18; 95% CI). For the  $Y_B$ -2012 period  
559 the mean EESC trend is +1.97 DU/year (+0.84 to +3.32 DU/year; 95% CI), and the mean  
560 PWLT trend is +3.18 DU/year (+1.66 to +4.74; 95% CI).

561 For the 1979- $Y_B$  period the distributions of EESC and PWLT trends (top panel) are  
562 rather similar, although the PWLT correlations show a larger peak towards high  
563 correlations compared to the EESC correlations (bottom panel). However, for the  $Y_B$ -  
564 2012 trends the probability distributions are very different (middle panel). The EESC  
565 trends show a tri-modal distribution, because only three different EESC curves were

566 used. These three EESC curves differ predominantly in their post-1997 EESC trends (see  
567 also Figure 3). In addition, the tri-modal EESC trend probability distribution for  $Y_B$ -2012  
568 (middle panel) shows that in the linear regression the EESC fit is determined by the 1979-  
569  $Y_B$  period more than by the  $Y_B$ -2012 period, as the pre-break trend distribution does not  
570 show the same tri-modal shape. This is not surprising because the trends for the 1979- $Y_B$   
571 period are larger and cover a longer period than for  $Y_B$ -2012.

572 The correlations distributions (lower panel) are similar for the lowest and highest  
573 correlations for both the EESC and PWLT regressions, but in the bulk of the distribution  
574 the PWLT results in systematically higher correlations than the EESC regressions.

575 The upper two panels of Figure 4 also include the 1979-1999 and 2000-2012 PWLT  
576 trends and  $2\sigma$  errors as reported in Table 32. The uncertainty range of the 2000-2012  
577 PWLT trend in Table 32 and the range in Figure 4 are quite similar. However, the  
578 uncertainty range of the 1979-1999 PWLT trend in Table 32 is considerably smaller. This  
579 shows that uncertainties in the 1979-1999 ozone trends are larger than estimated by a  
580 single regression estimated even though all 1979-1999 trends are statistically significant.

581 The auto-correlation of the ozone residuals is small (one-year lag values are  
582 approximately zero), indicating that the auto-correlation present in the ozone record (*e.g.*  
583 Fioletov and Shepherd, 2003; Vyushin et al., 2007) is related to some of the processes  
584 described by the regression parameters and are removed by the multi-multivariate  
585 regression. Auto-correlation thus does not have to be taken into account in the trend  
586 significance calculation.

587

### 588 **3.4 Regression model performance: sensitivity to the independent variables**

589

590 Sensitivities of the PWLT-based and EESC-based regressions to the ozone and EP flux  
591 scenarios are shown in Figure 5. PWLT-based regressions show that the PWLT  
592 distribution peak at high correlations is a consistent feature of different ozone records  
593 (*Sep-Nov, Sep-Oct, Sep, 7 Sep - 13 Oct, worst 30 days*). Similarly, use of several different  
594 EP fluxes also aligns with the PWLT correlation distribution peak, in particular the EP  
595 flux scenarios that include both the August and September months. For ozone,  
596 correlations get smaller for, respectively, the longest period (19 July – 1 December),  
597 shortest period (21-30 September) and October averages.

598 Figure 6 shows the probability distribution of volcanic aerosols for both the PWLT and  
599 EESC regressions. Volcanic aerosols have little impact on the explanatory power of the  
600 regression results, as already indicated by lack of correlation of this regressor with the  
601 ozone record. The PWLT regression coefficient values show that the effect of volcanic  
602 aerosols on total ozone can be either positive or negative, largely depending on the  
603 assumed amount of Pinatubo aerosols relative to El Chichón aerosols, although the  
604 distribution predominantly suggests positive regression values. The EESC regressions  
605 show a similar sign dependence of total ozone on volcanic aerosol, but with no clear sign  
606 of the regression value. None of other parameters (~~EP-FLUX- flux~~ scenario, Ozone  
607 scenario) have a sign-dependent effect on the aerosol regression coefficient value for both  
608 the EESC and PWLT scenarios. The strong sensitivity of the volcanic aerosol regression  
609 value – including sign changes – to either aerosol or EESC scenario indicates that  
610 including volcanic aerosols is not very important for the multivariate regression and  
611 better should be excluded altogether from multi-multivariate regressions due to

612 | insufficient information in the Antarctic total ozone record to constrain the total ozone –  
613 | volcanic aerosol relation.

614 | For the solar flux – QBO index (Figure 7, panel A) we find no clear dependence of  
615 | regression coefficient values on any of the scenarios or parameters. The probability  
616 | distributions for both the EESC and PWLT regressions are very similar. Hence, like for  
617 | volcanic aerosols, the solar-QBO parameter better should be excluded altogether from  
618 | ~~multi-multivariate~~ regressions because the Antarctic ozone record also contains  
619 | insufficient information to constrain the ozone – solar-QBO relation

620 | The SAM regression coefficient values show a continuous random distribution while  
621 | the overall dependence is predominantly negative (Figure 7, panel B). A positive phase of  
622 | the SAM correlates with more ozone depletion than a negative phase of the SAM. This is  
623 | a well-known two-way effect: tropospheric circulation changes affect Antarctic  
624 | stratospheric ozone on the short term, while the long term changes in Antarctic ozone  
625 | have affected the tropospheric circulation in the Southern Hemisphere [Kirtman et al.,  
626 | 2013; IPCC AR5, Ch. 11, section 11.3.2.4.2 and references therein].

627 | -For the EP-~~FLUX~~ flux the regressions show a positive dependence (Figure 7, panel C)  
628 | and a similar distribution for both the EESC and PWLT regression.

629 |

### 630 | **3.5 Optimal regressor and ozone record scenarios**

631 |

632 | Based on the analysis of the entire ensemble presented here it might be possible to  
633 | choose an optimal set of regressors as well as an optimal ozone record scenario for  
634 | Antarctic ozone trend analysis. Volcanic aerosols (Figure 6), the QBO and the solar cycle

635 (Figure 7) are shown to have little effect on the regression and thus better should be  
636 excluded. For the EP flux, it appears that including the months August and September  
637 leads to a better fit (higher correlations; Tables 54 and 65, Figure 5). For ozone, results  
638 suggest that there is no clear optimal time-window over which to calculate average  
639 ozone, but it appears that the period should not be too short, not be too long, and should  
640 include September and preferably the first half of October (Tables 54 and 65).

641 In addition, the use of three different EESC scenarios results in tri-modal distribution  
642 features in several parameters (Figures 43, middle panel and 6, lower panel), suggesting  
643 that care has to be taken with in particular the ozone trend values attributed to changes in  
644 EESC<sup>2</sup>s. Furthermore, the post-break trends are particularly sensitive to the choice in  
645 EESC scenario (Figure 3). It could therefore be argued that using a PWLT for post-break  
646 trend estimates is preferred over using the EESC-based post-break trend as its distribution  
647 better reflects structural uncertainties in the regression and takes the regression residuals  
648 into account for calculation of trend uncertainties.

649 Figure 8 illustrates what the best single regressions in the entire ensemble for all three  
650 regression models separately look like. The best EESC-regression correlation ( $R^2 = 0.95$ )  
651 was found for a case with Sep -Nov ozone, Jul-Aug EP flux and an EESC with an age-of-  
652 air of 4 years. For the best PWLT-regression correlation ( $R^2 = 0.96$ ) these were the same  
653 with 1997 as optimal break year. Reason for the high explanatory power is that in all  
654 three cases the specific SAM anomalies align with strong ozone peaks whereas the solar  
655 flux – QBO index variations coincidentally align with the smaller ozone anomalies.

656

657 **4. Discussion: Second stage of ozone recovery and trend significance.**

658

659       Given the broad range of outcomes for the different types of regressions and regressors,  
660 an important question is not only if ozone has started to increase after the late 1990s, but  
661 also whether the trend is statistically significant and can be attributed to declining  
662 stratospheric halogens, which is required by WMO for the second stage of ozone  
663 recovery to be formally identified. Because the EESC curve-shape is prescribed, there is  
664 no degree of freedom allowing for different pre-break and post-break trends in the EESC  
665 regression. As discussed in section 2, it is not clear *a priori* which EESC scenario is the  
666 optimal choice or if it is even appropriate to use just a single EESC scenario.  
667 Furthermore, as already discussed in section 3.1, the method for estimating the trend  
668 uncertainty of the post-BREAK trend for the EESC fit in Kuttippurath et al. [2013] is not  
669 justified, and Hence, how to assign an overall uncertainty to the EESC curve remains an  
670 open question. Therefore, a better-more appropriate approach would be to investigate  
671 whether the PWLT post-break trends are statistically significant as they use the ozone fit  
672 residuals for their significance calculation.

673       Figure 9 shows the probability distribution of correlations ( $R^2$ ) of the PWLT regression  
674 models vs. ozone for the entire Monte Carlo dataset, as well as the fraction of post-break  
675 PWLT trend estimates that are statistically significant ( $2\sigma$ ) for both the periods ending in  
676 2010 and 2012. This figure is comparable to Figure 4 (lower panel) and Figure 5, but  
677 with larger correlation bins for visualization purposes. Results indicate that trends only  
678 become statistically significant beyond a certain explanatory power of the regression  
679 model. This is not surprising: only when ozone residuals after removing the regression  
680 results are sufficiently small can the post-break trend become statistically significant.

681 This automatically requires a high correlation between the ozone record and the selected  
682 regression model. The analysis here shows that statistically significant trends require a  
683 correlation ( $R^2$ ) of at least approximately 0.60. Furthermore, only for high ozone-  
684 regression model correlations ( $R^2 > 0.80$ ) the majority of trends become statistically  
685 significant. In addition, the level of significance for the statistically significant trends is in  
686 most cases still less than  $3\sigma$  (not shown), indicating that a considerable amount of  
687 variability is not accounted for in the regression.

688 In section 3.5 the results of the ensemble were analyzed to determine optimal scenarios  
689 in terms of explanatory power ( $R^2$ ). However, the second stage of ozone recovery  
690 requires also a statistically significant post-break year trend. We therefore analyzed the  
691 percentage of statistically significant post-break trends in the ensemble for the PWLT-  
692 based regressions. We focus on the ozone record and EP flux scenarios as the  
693 uncertainties associated with these two parameters are the most important ones, as  
694 discussed before. Table 5 shows the percentage of regressions for each combination of  
695 ozone record and EP flux scenarios that is statistically significant for the ozone records  
696 ending in 2010. There are large differences in the fraction of statistically significant  
697 PWLT-based trends, ranging from less than 0.1% (*21-30 September average ozone*) to a  
698 complete 100% significance (*September-October* and *October ozone, 45S-75S Aug-Sep*  
699 *EP flux*). Table 6 shows the same results as Table 5, but only for the break year 1997 and  
700 the period ending in 2012. In this case there is a large number of ozone record - EP flux  
701 scenario combinations with statistically significant trends. If we would consider only the  
702 EP fluxes that include the August and September months, then with the exception of the  
703 *21-30 September* time window nearly all trends are statistically significant.



704 Excluding the year 2002 from the regressions has a significant impact on the post-break  
705 ordinary linear ozone trends without applying a multi-multivariate regression. However,  
706 it hardly has any effect on the post-break ordinary linear trends when including the  
707 ordinary linear trend in the multi-multivariate regressions (not shown), indicating that the  
708 multi-multivariate regression effectively removes the anomalous year 2002. Excluding  
709 volcanic years from the regression had no significant effect on both the ozone trends  
710 before and after the regression, consistent with our finding that there appears to be little  
711 (direct) impact of volcanic aerosols on Antarctic springtime total ozone. Note that  
712 Solomon et al. [2005] showed that volcanic effects can be seen in Antarctic ozone  
713 profiles during the ozone hole season – in particular in the UTLs region, but that the  
714 magnitude and vertical extent of the effects are too small to be detectable in total ozone  
715 column variations.

716 Table 7 shows the number of significant trends as function of the length of the period  
717 over which the trend is calculated. The number of significant trends varies between  
718 approximately 30-60%, and ~~that the number of significant trends further~~ depends on the  
719 choice of break year, with an overall increase in the number of statistically significant  
720 trends ~~increasing steadily~~ with increasing length of the period over which trends are  
721 calculated. This is not surprising as the regression trend error decreases with increasing  
722 number of points for which the trends are calculated (Supplementary Information  
723 equation S2). Furthermore, this implies that with continued extension of the total ozone  
724 record detection of Antarctic ozone recovery may be reached before 2020 using multi-  
725 multivariate regressions. Note that although in total the number of statistically significant  
726 trends increases with record length, this is not necessarily always the case: ~~(For example~~

727 ~~by comparing Table 5 and Table 6 — thus for it is concluded shows that for some scenario~~  
728 ~~combinations the number of significant trends is larger for a (shorter) period (BREAK-~~  
729 ~~2010) than for the full period vs. 1998-2012 trends).~~

730

731 ~~Excluding the year 2002 from the regressions has a significant impact on the post-break~~  
732 ~~ozone trends themselves. However, it hardly has any effect on the post-break trends from~~  
733 ~~the regressions (not shown), indicating effective removal of the anomalous year 2002~~  
734 ~~from the results. Excluding volcanic years from the regression had no significant effect~~  
735 ~~on both the ozone trends before and after the regression, consistent with our finding that~~  
736 ~~there appears to be little (direct) impact of volcanic aerosols on Antarctic springtime~~  
737 ~~ozone.~~

738 ~~It is tempting to interpret, based on some selections of our results, that the significance~~  
739 ~~is sufficient for identification of the second stage of ozone recovery by 2012. However,~~  
740 ~~comparing Table 5 and Table 6 — thus 2000-2010 trends vs 1998-2012 trends — shows~~  
741 ~~that the longer period not always results in increased statistical significance. In particular,~~  
742 ~~the need to average ozone over longer periods of time may introduce long-term changes~~  
743 ~~in average ozone that are not related to photochemical ozone destruction. Furthermore,~~  
744 ~~the tTrend significance is generally between  $2\sigma$  and  $3\sigma$  (not shown), indicating that a~~  
745 ~~considerable amount of variability is not accounted for in the regression. In addition, our~~  
746 ~~analysis shows sthat detection of the 2<sup>nd</sup>-stage of ozone recovery based on just one more~~  
747 ~~or less arbitrary selected (set of) regressor — ozone record combination(s) does not reflect~~  
748 ~~the structural uncertainties present in the underlying data.~~

749 | Nevertheless, the appearance of larger groups of statistically significant results  
750 | occurring for longer time series and a certain persistence among ozone scenarios and EP  
751 | flux scenarios; shows that ~~these type of multivariate regression, preferably using~~  
752 | piecewise linear analyses before and after a predefined break year, are capable of  
753 | removing deterministic variations in average ozone, and that with increasing length of the  
754 | post-break period more and robust statistically significant results can be expected.

755

## 756 | **5. Conclusions**

757

758 | The primary goal of this study was to investigate whether or not the 2<sup>nd</sup> stage of ozone  
759 | recovery – a statistical increase in ozone attributable to ozone depleting substances – can  
760 | be detected, given uncertainties in underlying data. A detailed sensitivity analysis of  
761 | widely used ~~multi-multi~~variate regression analysis of total ozone columns was presented  
762 | focusing on Antarctic springtime ozone. By combining regressor scenarios and Monte  
763 | Carlo simulations for various ozone record scenarios, a total of approximately 23 million  
764 | different multivariate regressions were performed.

765 | Our analysis shows that detection of the 2<sup>nd</sup> stage of ozone recovery based on one more  
766 | or less arbitrary selected (set of) regressor – ozone record combination(s) does not reflect  
767 | the structural uncertainties present in the underlying data.

768

769 | Use of the post-break trends based on fitting the EESC to the total ozone record is not  
770 | recommended, as these trends are solely based on the pre-defined EESC shape, ~~and~~ do  
771 | not allow flexibility in the trend calculation while it is unclear how to assign uncertainties

772 ~~to the EESC-regression-based trends in total ozone. Because the resulting EESC fit based~~  
773 ~~trend uncertainties do not take the ozone fit residuals into account the EESC scenarios~~  
774 ~~result in overconfident ozone trend uncertainties, neglecting structural uncertainties and~~  
775 ~~sensitivity to the chosen scenario.~~

776 Our analysis further shows that the EP flux and the SAM effects are capable to explain  
777 significant parts of Antarctic ozone variations and the removal of these effects improves  
778 the analysis of recovery, in contrast to the inclusion in the regressions of volcanic  
779 aerosols and the combined QBO/Solar flux index.

780 Consistent with expectations, we find a robust gradual small increase in Antarctic  
781 ozone since the late 1990s that can be attributed to decreases in ODS for selected  
782 combinations of regressors, although the magnitude of the increase is rather uncertain  
783 (+1.66  $\pm$  +4.74 DU/year; 95% CI). The trend significance shows a clear dependence on  
784 the length of the period over which the trend is calculated. The number of statistically  
785 significant trends in our ensemble varies between approximately 30-60%, depending on  
786 the length of the period, with an average of approximately 50%.

787 The limited information present in the Antarctic ozone record for volcanic aerosols  
788 (essentially two isolated peaks) is consistent with Knibbe et al. [2014], who found little  
789 evidence for volcanic effects on total ozone throughout the Southern Hemisphere.  
790 Furthermore, Poberaj et al. [2011] also reported little impact of volcanic aerosols from  
791 the Pinatubo eruption on Southern Hemispheric ozone, attributing it to dynamical  
792 conditions favoring more poleward transport of ozone from the tropics and mid-latitudes  
793 than usual, thereby “*overcompensating the chemical ozone loss ...and reduce the overall*  
794 *strength of the volcanic ozone signal*”.

795 The lack of correlation between Antarctic ozone and the solar-flux/QBO combined  
796 index was also found by Knibbe et al. [2014] for both Antarctic (and Arctic) ozone  
797 trends. This lack of QBO-solar signal in Antarctic springtime ozone – also e.g. reported  
798 in both Labitzke [2004] and Roscoe and Haigh [2007] - may be related to the dominance  
799 in absolute values of the ozone change of ozone depletion and vortex dynamics over  
800 potential indirect solar influences on Antarctic springtime ozone.

801 From our analysis it remains unclear what the appropriate time window would be over  
802 which to average the ozone record and the EP flux. Results indicate that the best  
803 regression occur for ozone averaged over a time window that includes the ozone hole  
804 season – typically September and part of October. On the other hand, the time window  
805 should also not extend far beyond the ozone hole season as more and more non-  
806 photochemical ozone variations are introduced in the averaged ozone with a longer  
807 averaging period. Similarly, for the EP flux we find that including both the August and  
808 September months result in the best regressions. However, the choice for using complete  
809 calendar months is rather arbitrary, and better choices may exist which is here left for  
810 future research.

811 The lack of a proper definition of appropriate time windows drives our recommendation  
812 that care has to be taken with drawing firm conclusions about Antarctic ozone recovery  
813 based on ~~multi-multi~~variate regression of Antarctic vortex average ozone. Given  
814 uncertainties in parameters and independent variables and choices in defining the optimal  
815 time period and area for calculating the ozone record and the independent variables ~~It~~ is  
816 tempting to discard those results ~~in the full ensemble~~ that do not confirm our  
817 expectations, but without proper justification of what constitutes the best set of

818 independent explanatory variables – for example physically compelling arguments - there  
819 is the danger of working towards an expected answer.

820 ~~Another last finding is that~~Finally, a longer post-break period does not necessarily  
821 ~~always results in more significant trends, which provides yet another indication to remain~~  
822 ~~careful with drawing too firm conclusions from multivariate regressions. On the other~~  
823 ~~hand~~despite these uncertainties, our results indicate it can be expected that with extending  
824 the ozone record and using a multi-multivariate regression method to remove well-  
825 selected non-ODS influences from the total ozone record – the second stage of recovery  
826 of the Antarctic ozone-hole ~~will~~may be detectable before 2020. Future updates of the  
827 analysis in this paper by extension of the present-day ozone records are expected ~~will~~  
828 ~~rather soon~~ provide indications whether this moment approaches fast or not.

829

830

831 **Acknowledgements**

832 The authors wish to thank the following authors of chapter 3 of the 2014 WMO ozone  
833 assessment report – Sophie Godin Beekmann, Martin Dameris, Peter Braesicke, Martin  
834 Chipperfield, Markus Rex and Michelle Santee – as well as John Pyle, Ted Shepherd and  
835 in particular Paul Newman for encouraging us to write this paper.

836

837 **References**

838

839 Van der A et al. (2010), Multi sensor reanalysis of total ozone *Atm. Chem. Phys.*, 10,  
840 11277-11294, doi:10.5194/acp-10-11277-2010.

841 Ammann et al. (2003), A monthly and latitudinally varying volcanic forcing dataset in  
842 simulations of 20th century climate, *Geophys. Res. Lett.*, 30, 1657,  
843 doi:10.1029/2003GL016875.

844 Andrews et al. (1987), *Middle Atmosphere Dynamics*, Academic Press, Orlando, Florida,  
845 489 pp.

846 Anet et al. (2013), Impact of a potential 21st century “grand solar minimum” on surface  
847 temperatures and stratospheric ozone, *Geophys. Res. Lett.*, 40, 4420–4425,  
848 doi:10.1002/grl.50806.

849 Bekki et al., (2011), Future Ozone and its impact on surface UV, Chapter 3 Scientific  
850 Assessment of Ozone Depletion: 2010, Global Ozone Research and Monitoring  
851 Project - Report No. 52, 516 pp., Geneva, Switzerland.

852 Bunzel and Schmidt (2013), The Brewer–Dobson Circulation in a Changing Climate:  
853 Impact of the Model Configuration. *J. Atmos. Sci.*, 70, 1437–1455. doi:  
854 <http://dx.doi.org/10.1175/JAS-D-12-0215.1>

855 Crowley and Unterman (2012), Technical details concerning development of a 1200-yr  
856 proxy index for global volcanism, *Earth Syst. Sci. Data Discuss.*, 5, 1-28,  
857 doi:10.5194/essdd-5-1-2012.



858 Dameris, M., S. Matthes, R. Deckert, V. Grewe, and M. Ponater (2006), Solar cycle  
859 effect delays onset of ozone recovery, *Geophys. Res. Lett.*, 33, L03806,  
860 doi:[10.1029/2005GL024741](https://doi.org/10.1029/2005GL024741).

861 De Laat and van Weele, (2011) The 2010 Antarctic ozone hole: Observed reduction in  
862 ozone destruction by minor sudden stratospheric warmings, *Sci. Rep.*, 1, 38, doi:  
863 10.1038/srep00038.

864 Dudok de Wit et al. (2009), Finding the best proxies for the solar UV irradiance,  
865 *Geophys. Res. Lett.*, 36, L10107, doi:10.1029/2009GL037825.

866 Ebdon (1960): Notes on the wind flow at 50 mb in tropical and sub-tropical regions in  
867 January 1957 and January 1958. *Q. J. Roy. Met. Soc.*, 86, 540-542.

868 Engel et al. (2009), Age of stratospheric air unchanged within uncertainties over the past  
869 30 years, *Nature Geoscience* 2, 28 – 31, doi:10.1038/ngeo388.

870 Eyring, et al. (2007), Multimodel projections of stratospheric ozone in the 21st century, *J.*  
871 *Geophys. Res.*, 112, D16303, doi:10.1029/2006JD008332.

872 Fioletov, V. E., and T. G. Shepherd (2003), Seasonal persistence of midlatitude total  
873 ozone anomalies, *Geophys. Res. Lett.*, 30, 1417, doi:[10.1029/2002GL016739](https://doi.org/10.1029/2002GL016739).

874 Graystone (1959), Meteorological office discussion on tropical meteorology. *Met.*  
875 *Magazine*, 88, 117.

876 Haigh, J.D., The impact of solar variability on climate (1996), *Science*, Vol. 272, no.  
877 5264 pp. 981-984, DOI: 10.1126/science.272.5264.981

878 Haigh and Roscoe (2006), Solar influences on polar modes of variability,  
879 *Meteorologische Zeitschrift*, Volk.15, pp. 371-378

880 Ho et al. (2012) The Southern Annular Mode: a comparison of indices, *Hydrol. Earth*  
881 *Syst. Sci.*, 16, 967-982, doi:10.5194/hess-16-967-2012.

882

883 Hood, L. (1997), The solar cycle variation of total ozone: Dynamical forcing on the lower  
884 stratosphere, *Journal of Geophysical Research*, 102(D1), 1355-1370.

885 Huang and Massie (1997), Effect of volcanic particles on the O<sub>2</sub> and O<sub>3</sub> photolysis rates  
886 and their impact on ozone in the tropical stratosphere, *J. Geophys. Res.*, 102(D1),  
887 1239–1249, doi:10.1029/96JD02967.

888 Jiang et al. (2008): Interannual Variability and Trends of Extratropical Ozone. Part II:  
889 Southern Hemisphere. *J. Atmos. Sci.*, 65, 3030–3041, doi: 10.1175/2008JAS2793.1

890 Kalnay, E., et al. (1996). The NCEP/NCAR 40-Year Reanalysis Project, *Bull. Am. Met.*  
891 *Soc.*, **77** (3): 437–471.

892 Kirtman et al. (2013), Near-term Climate Change: Projections and Predictability. In:  
893 *Climate Change 2013: The Physical Science Basis. Contribution of Working Group I*  
894 *to the Fifth Assessment Report of the Intergovernmental Panel on Climate Change,*  
895 *Stocker et al. (EDS.), Cambridge University Press, Cambridge, United Kingdom and*  
896 *New York, NY, USA, in press.*

897 Klekociuk et al. (2011), The Antarctic ozone during 2010, *Australian Meteorological and*  
898 *Oceanographic Journal*, 61 (4), 253-267.

899 Knibbe, J. S., et al. (2014), Spatial regression analysis on 32 years of total column ozone  
900 data, *Atmos. Chem. Phys.*, 14, 8461-8482, doi:10.5194/acp-14-8461-2014,.

901 Kramarova et al. (2014), Measuring the Antarctic ozone hole with the new Ozone  
902 Mapping and Profiler Suite (OMPS), *Atmos. Chem. Phys.*, 14, 2353-2361,  
903 doi:10.5194/acp-14-2353-2014.

904 Kuttippurath et al. (2010), Estimation of Antarctic ozone loss from ground-based total  
905 column measurements, *Atmos. Chem. Phys.*, 10, doi: 10.5194/acp-10-6569-2010,  
906 6569-6581.

907 Kuttippurath et al., Antarctic ozone loss in 1979–2010 (2013) first sign of ozone  
908 recovery, *Atmos. Chem. Phys.*, 13, doi: 10.5194/acp-13-1625-2013, 1625-1635,.

909 Labitzke (2004), On the signal of the 11-Year sunspot cycle in the Stratosphere over the  
910 Antarctic and its modulation by the Quasi-Biennial Oscillation (QBO),  
911 *Meteorologische Zeitschrift*, Vol. 13, No. 4, 263-270.

912 McCormack, J. P., & Hood, L. L. (1996). Apparent solar cycle variations of upper  
913 stratospheric ozone and temperature: Latitude and seasonal dependences. *Journal of*  
914 *Geophysical Research: Atmospheres*, 101(D15), 20933-20944.

915 Naujokat (1986), An update of the observed quasi-biennial oscillation of the stratospheric  
916 winds over the tropics. *J. Atmos. Sci.*, 43, 1873-1877.

917 Newman et al. (2006), When will the Antarctic ozone hole recover? *Geophys. Res. Lett.*,  
918 33, L12814, doi:10.1029/2005GL025232.

919 Newman et al. (2007), A new formulation of equivalent effective stratospheric chlorine  
920 (EESC), *Atmos. Chem. Phys.*, 7, 4537-4552, doi:10.5194/acp-7-4537-2007.

921 Poberaj et al. (2011): Missing Stratospheric Ozone Decrease at Southern Hemisphere  
922 Middle Latitudes after Mt. Pinatubo: A Dynamical Perspective. *J. Atmos. Sci.*, 68,  
923 1922–1945. doi: <http://dx.doi.org/10.1175/JAS-D-10-05004.1>

924 Randel et al. (2002), Changes in column ozone correlated with the stratospheric EP flux,  
925 J. Meteor. Soc. Jap., 80, 4b, 849-862.  
926

927 Rozanov et al. (2002), Climate/chemistry effects of the Pinatubo volcanic eruption  
928 simulated by the UIUC stratosphere/troposphere GCM with interactive  
929 photochemistry, J. Geophys. Res., 107(D21), 4594, doi:10.1029/2001JD000974.

930 Salby et al. (2011), Rebound of Antarctic ozone, *Geophys. Res. Lett.*, 38, L09702, doi:  
931 10.1029/2011GL047266.

932 Salby et al. (2012), Changes of the Antarctic ozone hole: Controlling mechanisms,  
933 seasonal predictability, and evolution, *J. Geophys. Res.*, 117, D10111, doi:  
934 10.1029/2011JD016285.

935 Sato et al. (1993), Stratospheric aerosol optical depths, 1850-1990. *J. Geophys. Res.*, 98,  
936 22987-22994, doi:10.1029/93JD02553.

937 [Solomon, S. et al. \(2005\), Four decades of ozonesonde measurements over Antarctica, J.](#)  
938 [Geophys. Res., 110, D21311, doi:10.1029/2005JD005917.](#)

939 Solomon, S., et al. (2011), The persistently variable “background” stratospheric aerosol  
940 layer and global climate change. *Science*, Vol. 333, no. 6044, pp. 866-870, doi:  
941 10.1126/science.1206027

942 Soukharev and Hood (2006), Solar cycle variation of stratospheric ozone: Multiple  
943 regression analysis of long-term satellite data sets and comparisons with models, *J.*  
944 *Geophys. Res.*, 111, D20314, doi:10.1029/2006JD007107.

945 Stiller et al. (2008), Global distribution of mean age of stratospheric air from MIPAS SF6  
946 measurements, *Atmos. Chem. Phys.*, 8, 677-695, doi:10.5194/acp-8-677-2008.

947 Telford et al. (2009), Reassessment of causes of ozone column variability following the  
948 eruption of Mount Pinatubo using a nudged CCM, *Atmos. Chem. Phys.*, 9, 4251-  
949 4260, doi:10.5194/acp-9-4251-2009, 2009.

950 Thompson, D.W.J. and J.M. Wallace (2000): Annular Modes in the Extratropical  
951 Circulation, Part I: Month-to-Month Variability, *J. Climate*, 13, 1000–1016.

952

953 United Nations Environment Programme (2012), *The Montreal Protocol on Substances*  
954 *that Deplete the Ozone Layer*, Nairobi, Kenya, ISBN 978-9966-20-009-9.

955 Vernier, J.-P., et al. (2011), Major influence of tropical volcanic eruptions on the  
956 stratospheric aerosol layer during the last decade, *Geophys. Res. Lett.*, 38, L12807,  
957 doi:10.1029/2011GL047563.

958 Vyushin, D., V. E. Fioletov, and T. G. Shepherd (2007), Impact of long-range  
959 correlations on trend detection in total ozone, *J. Geophys. Res.*, 112, *D14307*,  
960 doi:[10.1029/2006JD008168](https://doi.org/10.1029/2006JD008168)

961 Weber et al. (2003), Dynamical control of NH and SH winter/spring total ozone from  
962 GOME observations in 1995-2002, *Geophys. Res. Lett.*, 30, 1853, doi:  
963 10.1029/2002GL016799.

964 Weber et al. (2011), The Brewer-Dobson circulation and total ozone from seasonal to  
965 decadal time scales, *Atmos. Chem. Phys.*, 11, 11221-11235, doi: 10.5194/acp-11-  
966 11221-2011.

967 World Meteorological Organization (2007), *Scientific Assessment of Ozone Depletion:*  
968 *2006*, Global Ozone Research and Monitoring Project - Report No. 50, 572 pp.,  
969 Geneva, Switzerland.

970 World Meteorological Organization (2011), Scientific Assessment of Ozone Depletion:  
971 2010, Global Ozone Research and Monitoring Project - Report No. 52, 516 pp.,  
972 Geneva, Switzerland.

973 | Yang, E.-S., D. M. Cunnold, M. J. Newchurch, R. J. Salawitch, M. P. McCormiack, J. M.  
974 Russell III, J. M. Zawodny, and S. J. Oltmans (2008), First stage of Antarctic ozone  
975 recovery, *J. Geophys. Res.*, 113, D20308, doi:[10.1029/2007JD009675](https://doi.org/10.1029/2007JD009675).

976

977Tables

<p><b>EP flux</b></p> <p><a href="http://www.awi.de/en/research/research_divisions/climate_science/atmospheric_circulations_old/projects/candidoz/ep_flux_data/">http://www.awi.de/en/research/research_divisions/climate_science/atmospheric_circulations_old/projects/candidoz/ep_flux_data/</a></p>
<p><b>QBO</b></p> <p><a href="http://www.geo.fu-berlin.de/met/ag/strat/produkte/qbo/">http://www.geo.fu-berlin.de/met/ag/strat/produkte/qbo/</a></p>
<p><b>Solar flux</b></p> <p><a href="ftp://ftp.geolab.nrcan.gc.ca/data/solar_flux/monthly_averages/solflux_monthly_average.txt">ftp://ftp.geolab.nrcan.gc.ca/data/solar_flux/monthly_averages/solflux_monthly_average.txt</a></p>
<p><b>SAM</b></p> <p><a href="ftp://ftp.cpc.ncep.noaa.gov/cwlinks/">ftp://ftp.cpc.ncep.noaa.gov/cwlinks/</a></p>
<p><b>EESC</b></p> <p><a href="http://acdb-ext.gsfc.nasa.gov/Data_services/automailer/">http://acdb-ext.gsfc.nasa.gov/Data_services/automailer/</a></p>
<p><b>Volcanic aerosol</b></p> <p><a href="http://data.giss.nasa.gov/modelforce/strataer/">http://data.giss.nasa.gov/modelforce/strataer/</a></p>
<p><b>Assimilated total ozone</b></p> <p><a href="http://www.temis.nl/protocols/O3global.html">http://www.temis.nl/protocols/O3global.html</a></p>

978 **Table 1.** Data sources

979

<b>regressor</b>	<b>variations</b>
<p>Average EP flux - 8 scenarios</p>	<ul style="list-style-type: none"> <li>- 70 hPa, 40°S-90°S, Aug-Sep (baseline)</li> <li>- 70 hPa, 40°S-90°S, Jul-Aug</li> <li>- 70 hPa, 40°S-90°S, Jul-Sep</li> <li>- 70 hPa, 40°S-90°S, Jul</li> <li>- 70 hPa, 40°S-90°S, Aug</li> <li>- 70 hPa, 40°S-90°S, Sep</li> <li>- 70 hPa, 45°S-75°S, Aug-Sep</li> <li>- 100 hPa, 40°S-90°S, Aug-Sep</li> </ul>
<p>Solar flux – QBO index - 100 Monte Carlo series</p>	<ul style="list-style-type: none"> <li>- Random variations in Solar flux – QBO anomalies</li> <li>- 200% Gaussian noise variations on single solar flux – QBO anomalies</li> </ul>

SAM index - 100 Monte Carlo series	- 100% random error on annual mean SAM index values
EESC loading - 3 scenarios	- EESC shapes based on different age of air of 2.5, 4.0 and 5.5 years
Volcanic aerosol - 6 scenarios	<ul style="list-style-type: none"> <li>- Baseline Volcanic Aerosol index (NASA GISS)</li> <li>- Pinatubo peak scaled to El Chichón peak</li> <li>- Pinatubo peak 2.5 times the El Chichón peak</li> <li>- Pinatubo peak 5 times the El Chichón peak</li> <li>- El Chichón peak shifted one year back compared to Pinatubo peak</li> <li>- Pinatubo peak shifted one year back compared to El Chichón peak</li> </ul>
Ozone record - 8 scenarios	<ul style="list-style-type: none"> <li>- Sep-Oct-Nov average ozone (baseline)</li> <li>- Sep-Oct average ozone</li> <li>- Sep average ozone</li> <li>- Oct average ozone</li> <li>- 7 Sep – 13 Oct average ozone</li> <li>- Very short 21-30 Sep average ozone</li> <li>- Very long 19 Jul – 1 Dec average ozone</li> <li>- “Worst” 30-day average ozone.</li> </ul>

980 **Table 2.** Summary of the uncertainties for the proxies discussed in section 2.1 to 2.9 and

981 their inclusion in the regression analysis in this study.

982



Period	Kuttippurath et al. [2013]		This study	
	EESC	PWLT	EESC	PWLT
1979-1999	-4.50 ± 0.65	-5.02 ± 1.11	-5.39 ± 0.97 <del>22</del>	-5.66 ± 1.03
2000-2010	1.11 ± 0.16	2.91 ± 2.73	1.04 ± 0.19 <del>2</del>	3.30 ± 2.85
1979-1999			-5.26 ± 1.02 <del>0.21</del>	-5.75 ± 1.00
2000-2012			1.09 ± 0.23 <del>10</del>	3.28 ± 2.49

983 **Table 3.** EESC-based Antarctic vortex core ozone trends and their  $2\sigma$  trend uncertainties  
984 (DU/year) derived from ~~multi-~~multivariate linear regression. The trends in ozone based on  
985 EESC regression are calculated by an Ordinary Linear Regression based of the pre-  
986 defined change in EESC multiplied with the EESC regression coefficient for the time  
987 period under consideration [*cf.* Kuttippurath et al., 2013]. The EESC trend is in pptv/year,  
988 the EESC regression coefficient is in DU/pptv, hence the trend in ozone is in DU/year,  
989 allowing direct comparison with the PWLT ozone trends (also in DU/year)  
990

	EP- flux	EESC	AEROSOL	SF×QBO
SAM	-0.31 ± 0.27	-0.03 ± 0.17	-0.09 ± 0.19	-0.09 ± 0.29
SF×QBO	0.08 ± 0.28	0.07 ± 0.42	-0.02 ± 0.19	
AEROSOL	0.05 ± 0.17	0.03 ± 0.30		
EESC	0.25 ± 0.17			

991 **Table 4.** Cross correlations and their  $2\sigma$  variance between explanatory variables.  
992

EP flux \ Ozone									
		Aug - Sep	Jul - Aug	Jul - Sep	Jul	Aug	Sep	45°S-75°S	100 hPa
Sep - Nov		27.7	16.9	43.5	2.3	18.2	2.6	84.9	70.7
Sep - Oct		<b>98.5</b>	80.7	<b>99.7</b>	37.5	71.5	71.2	<b>100.0</b>	<b>100.0</b>
Sep		34.8	23.1	41.9	5.0	23.0	15.0	60.8	60.4
Oct		<b>99.4</b>	72.5	<b>99.2</b>	35.2	63.7	77.6	<b>100.0</b>	<b>99.9</b>
21 - 30 Sep		<0.1	<0.1	<0.1	<0.1	<0.1	<0.1	1.0	1.9
7 Sep - 13 Oct		54.3	19.5	55.2	5.3	17.8	24.4	92.1	90.7
Worst 30 days		87.3	52.9	94.2	18.8	42.2	53.6	<b>99.6</b>	<b>99.1</b>
19 Jul - 1 Dec		30.1	21.8	36.3	4.6	27.4	5.3	78.6	68.2

993 **Table 5.** Percentage of statistically significant regressions for each combination of ozone  
994 and EP flux scenarios, as defined in section 2, based on the PWLT regression model [for](#)  
995 [the all-break years 1997, 1998, and 1999, and all ending in 2010.](#) Each ensemble consists  
996 of results of 180,000 single regressions (6 volcanic aerosol scenarios, 100 SAM and 100  
997 QBO-solar index Monte Carlo runs, 3 break years). Numbers in bold are statistically  
998 significant > 95%.  
999

EP flux \ Ozone									
		Aug - Sep	Jul - Aug	Jul - Sep	Jul	Aug	Sep	45°S-75°S	100 hPa
Sep - Nov		<b>99.9</b>	10.7	92.6	0.1	36.3	29.5	<b>100.0</b>	<b>100.0</b>
Sep - Oct		<b>100.0</b>	52.2	<b>100.0</b>	4.2	73.4	<b>100.0</b>	<b>100.0</b>	<b>100.0</b>
Sep		<b>100.0</b>	40.3	<b>99.5</b>	2.0	67.5	96.4	<b>100.0</b>	<b>100.0</b>
Oct		<b>100.0</b>	12.1	<b>98.0</b>	0.6	27.2	<b>98.1</b>	<b>100.0</b>	<b>100.0</b>
21 - 30 Sep		0.1	<0.1	<0.1	<0.1	<0.1	<0.1	2.0	20.9
7 Sep - 13 Oct		<b>100.0</b>	10.0	<b>97.7</b>	0.8	19.6	<b>98.4</b>	<b>100.0</b>	<b>100.0</b>
Worst 30 days		<b>100.0</b>	20.0	<b>99.4</b>	1.2	29.6	<b>99.7</b>	<b>100.0</b>	<b>100.0</b>
19 Jul - 1 Dec		<b>99.9</b>	25.6	<b>95.3</b>	1.5	66.1	56.5	<b>100.0</b>	<b>100.0</b>

1000 **Table 6.** As table 5 but for the break year 1997 and the period ending in 2012.

1001

Start year	End year	Length (years)	significant trends
2000	2010	11	34.3%
1999	2010	12	47.8%
1998	2010	13	59.5%
all	2010		47.3%
2000	2012	13	39.0%
1999	2012	14	52.7%
1998	2012	15	60.7%
all	2012		50.5%

1002 **Table 7.** Fraction of statistically significant trends (%) in all regression results for  
1003 different break years, period lengths and different types of trend calculations. The start  
1004 year and end year refer to the time period for which trends are calculated. The “all” start  
1005 years refers to the statistics for all three start years scenarios combined.

1006

1007 **Supplementary information**

1008

1009

1010 **QBO.**

1011

1012 The Quasi-Biennial Oscillation (QBO) of the winds in the equatorial stratosphere has  
1013 been discovered in the 1950s through the establishment of a global, regularly measuring  
1014 radiosonde network [Graystone, 1959; Ebdon, 1960]). The Free University of Berlin has  
1015 compiled a long-term record from 1953 onwards of daily wind observations of selected  
1016 stations near the equator. From these daily measurements monthly mean zonal  
1017 components were calculated for pressure levels of 70, 50, 40, 30, 20, 15, and 10 hPa. For  
1018 the period after 1979 only measurements from Singapore are used. The QBO data set is  
1019 supposed to be representative of the equatorial belt since various studies have shown that  
1020 longitudinal differences in the phase of the QBO are small [Hood, 1997]. It should be  
1021 noted, however, that some uncertainties arose at higher levels during the early years from  
1022 the scarcity of observations. More information on the original data and their evaluation  
1023 can be found in Naujokat [1986].

1024 As proxy for the regressions we will use the 40-hPa QBO index, also used in  
1025 Kuttippurath et al. [2013]. Salby et al. [2011, 2012] chose to use 30-hPa winds instead.  
1026 Typical maximum zonal wind speeds are 20-30 m/s. -The relevancy of the choice of  
1027 QBO index will be evaluated later. Information on the uncertainties in the monthly QBO  
1028 data is not available. One indirect method to estimate the uncertainties is by examining  
1029 QBO index variability close to the maximum and minimum of the QBO cycles, where the  
1030 QBO index values remains more or less constant for some months. Assuming that during  
1031 the maximum or minimum in the QBO phase variations from month to month are

1032 indicative of uncertainties in the QBO, we come up with estimated uncertainties of  
1033 around 1.5-2.0 m/s in the zonal mean wind speeds.

1034

1035 **Solar flux**

1036

1037 Variations in incoming solar radiation – in particular the shorter ultraviolet wavelengths  
1038 – have an effect on stratospheric ozone [Haigh, 1996; McKormack and Hood, 1996;  
1039 Soukharev and Hood, 2006; Anet et al., 2013]. A standard proxy for variations in  
1040 incoming solar radiation in ozone regression studies is to use the monthly mean 10.7 cm  
1041 radio flux, as also used in Kuttippurath et al. [2013]. This data set was obtained via  
1042 NOAA/NESDIS/NGDC/STP.

1043 However, there are other solar activity proxies available. Ideally, in absence of true UV  
1044 spectral measurements, one would like to use a proxy that is representative for solar  
1045 activity at those wavelengths where stratospheric ozone formation occurs, which is of  
1046 roughly between 200 and 300 nm. Dudok de Wit et al. [2009] tried to identify the best  
1047 proxy for solar UV irradiance, and concluded that proxies derived from a certain  
1048 wavelength range best represent the irradiance variations in that wavelength band. Thus,  
1049 the 10.7-cm radio flux might not fully represent solar UV variability. Using the results  
1050 from Dudok and de Wit et al. [2009] to analyze a set of seven solar activity proxies  
1051 dating back to at least 1979 based on the solar2000 model and obtained from  
1052 NOAA/NESDIS/NGDC/STP (F10.7, Lyman-alpha, E10.7, and the solar constant S), we  
1053 will assume in our regressions that the uncertainty range associated with the solar proxy  
1054 is approximately 15% of the root-mean-square of the anomaly values.

1055

1056 **Why do standard errors of an ordinary linear regression relative to the regression**  
1057 **slope not depend on the actual regression itself?**

1058

1059 This analysis is based on the “Data Analysis Toolkit” document (chapter 10), written by  
1060 Prof. James Kircher, Professor of Earth and Planetary Science at the University of  
1061 California, Berkley and emeritus Goldman Distinguished Professor for the Physical  
1062 Sciences.

1063

1064 <http://seismo.berkeley.edu/~kirchner/>

1065

1066 The standard error of the regression slope **b** of an ordinary linear regression of two  
1067 variables **x** and **y**, and the regression slope **b** itself can be written as:

1068

1069 
$$s_b = \frac{b}{\sqrt{n-2}} \sqrt{\frac{1}{r^2} - 1} \quad \text{and} \quad b = r \frac{S_y}{S_x} \quad (\text{S1})$$

1070 In which **s<sub>b</sub>** is the standard error of the regression slope, **n** the number of data points of  
1071 the variables **x** and **y**, **r** is the Pearson correlation coefficient between the variables **x** and  
1072 **y**, and **S<sub>x,y</sub>** is the standard deviation of the variables **x** and **y**.

1073 For a statistically significant trend one generally defines that the trends (slopes) should  
1074 exceed two times the standard error. Or, in other words, the standard error of the  
1075 regression slope divided by the regression slope itself should be less than 0.5

1076 The standard error of the regression slope relative to the regression slope itself – which  
1077 directly relates to statistical significance of the trend - becomes, based on the equation  
1078 above:

1079 
$$s_b / b = \frac{1}{\sqrt{n-2}} \sqrt{\frac{1}{r^2} - 1} \quad (\text{S2})$$

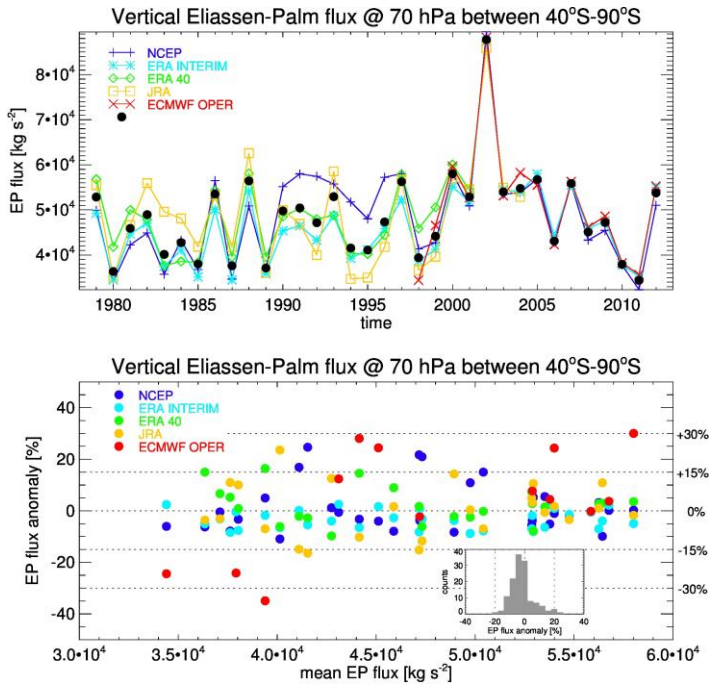
1080 which only depends on the correlation between the variables **x** and **y** and the number of  
1081 data points of variable **x** and **y** (record length).

1082



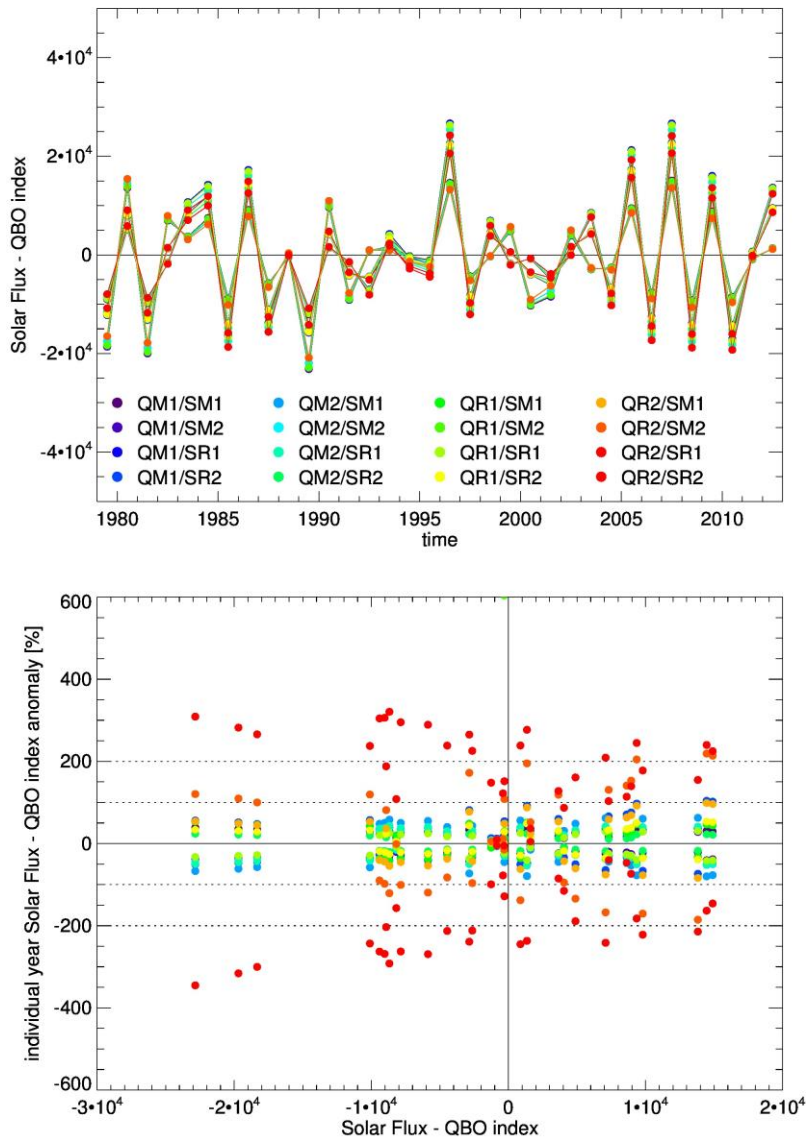
1 **Figures**

2



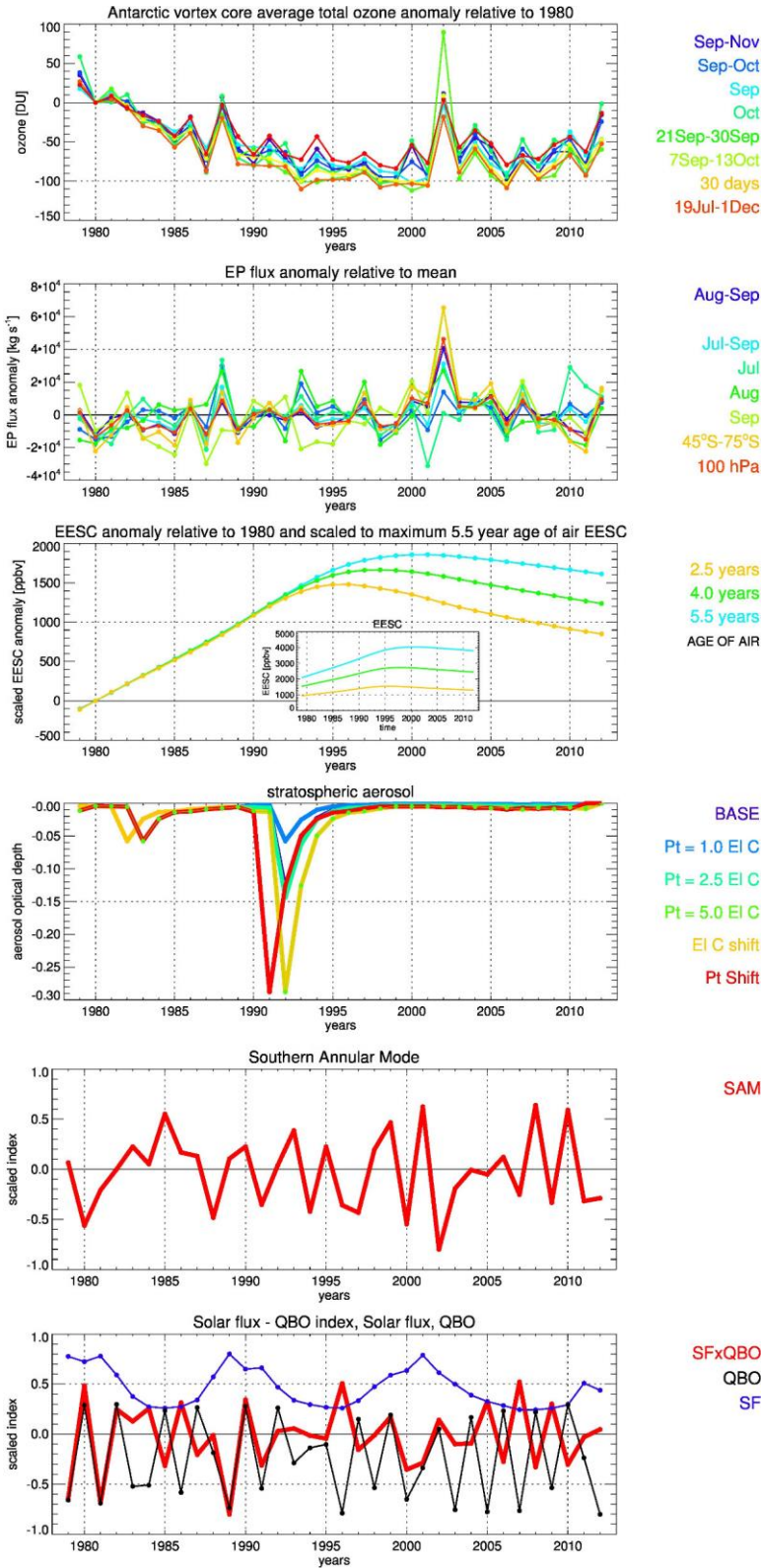
3

4 **Figure 1.** Vertical Eliassen-Palm (EP; kg/s<sup>2</sup>) flux at 70 hPa between 40°S and 90°S for  
5 five different meteorological datasets for the period 1979-2012 averaged for the two  
6 month period August-September: NCEP reanalysis 1979-2012, ECMWF ERA INTERIM  
7 1979-2012, ECMWF ERA 40 1979-2001, Japan Reanalysis 1979-2005, ECMWF  
8 operational analysis 1998-2012. Top panel shows the EP flux as function of time,  
9 including the mean EP flux for each year based on all datasets. Bottom panel shows the  
10 EP flux anomalies (%) of a given year as function of the mean EP flux (black dots in the  
11 upper panel) for all meteorological datasets available for that year. The insert shows the  
12 probability distribution of the relative anomalies. Data are obtained from the EP flux data  
13 website of the Alfred Wegener Institute (AWI) for Polar and Marine Research in  
14 Bremerhaven, Germany.

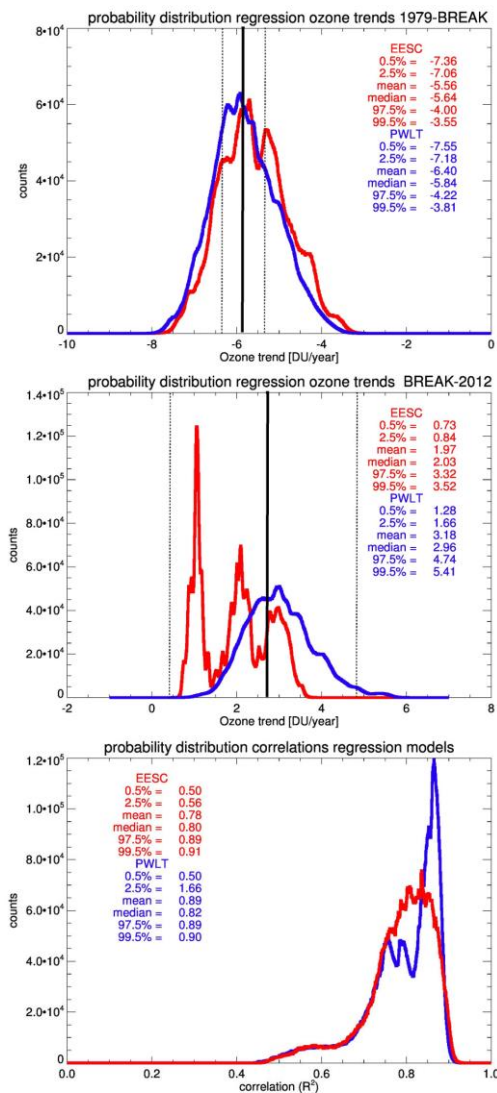


15

16 **Figure 2.** Time series of the combined Solar flux- QBO index (arbitrary units) (upper  
 17 plot) and the index anomalies relative to the average of different possibilities to derive at  
 18 the index. The Solar flux (“S”) and QBO (“Q”) anomalies were calculated based both on  
 19 the average (“M”) as well as the range of Solar flux and QBO values (“R”, see section 2.5  
 20 for the explanations of the “range”), and for both the entire record of Solar flux and QBO  
 21 values (1947-2012 and 1953-2012, respectively; “1”) as well as for the period 1979-2012  
 22 (“2”), resulting in a total of 16 combinations. The different colors denote the different  
 23 combinations.

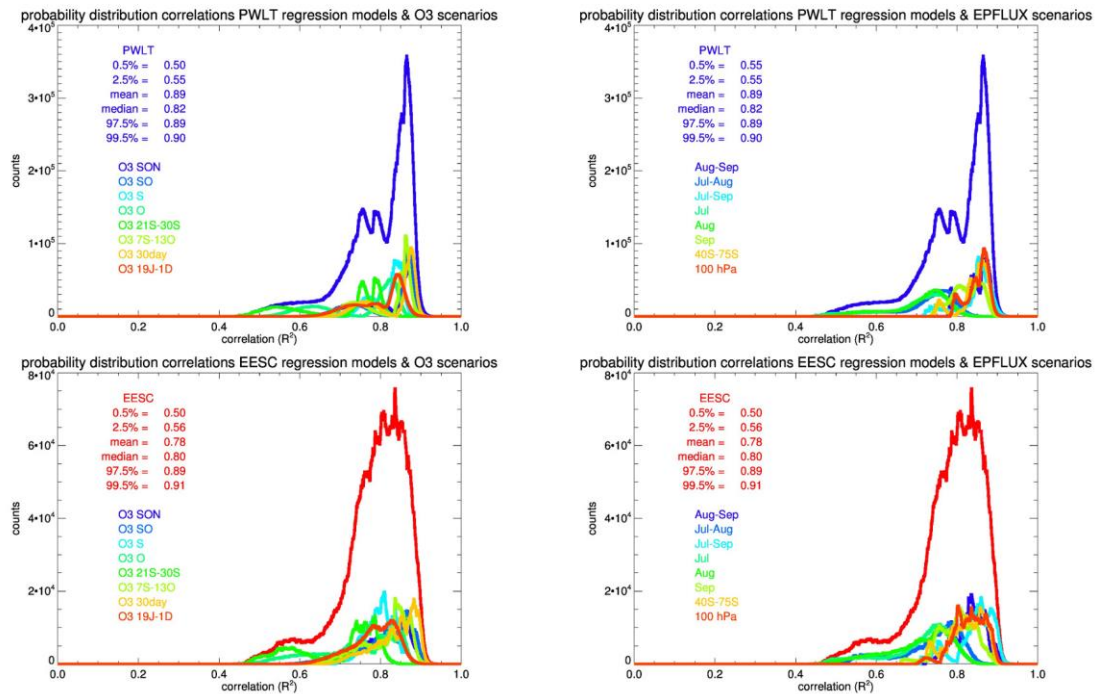


26 **Figure 3.** Time series of regressors for the period 1979-2012. For ozone, EP flux, EESC  
 27 and stratospheric aerosol all scenarios as defined in section 2 are included (indicated by  
 28 the different colors). For the SAM and the solar flux - QBO index only the baseline time  
 29 series is shown, and both indices – being unitless to start with - are scaled for proper  
 30 comparison. Ozone values are in DU, EP fluxes are in kg/s, EESC values are in ppbv and  
 31 stratospheric aerosol is in optical depth.



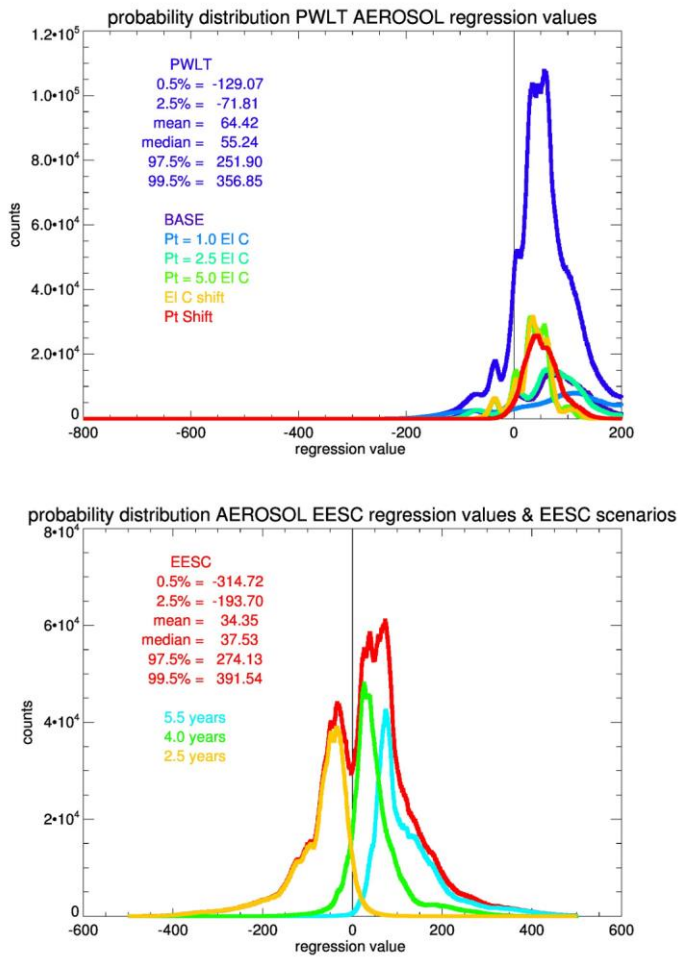
32  
 33 **Figure 4.** Probability distribution of ozone trends for the period 1979-break (upper plot)  
 34 and break-2012 (middle plot) as well as time correlations ( $R^2$ ) for the regression models

35 and the ozone record scenarios (lower plot). The colors indicate the distributions for the  
 36 two different long-term ozone regressions (EESC, PWLT). Indicated in the figure are  
 37 also the 0.5%-2.5%-mean-median-97.5%-99.5% probability values of trends and  
 38 correlations. The vertical black lines in the upper two panels indicate the trend (solid) and  
 39  $2\sigma$  errors (dotted) of the PWLT regression results of table 2 for the period 2000-2012.



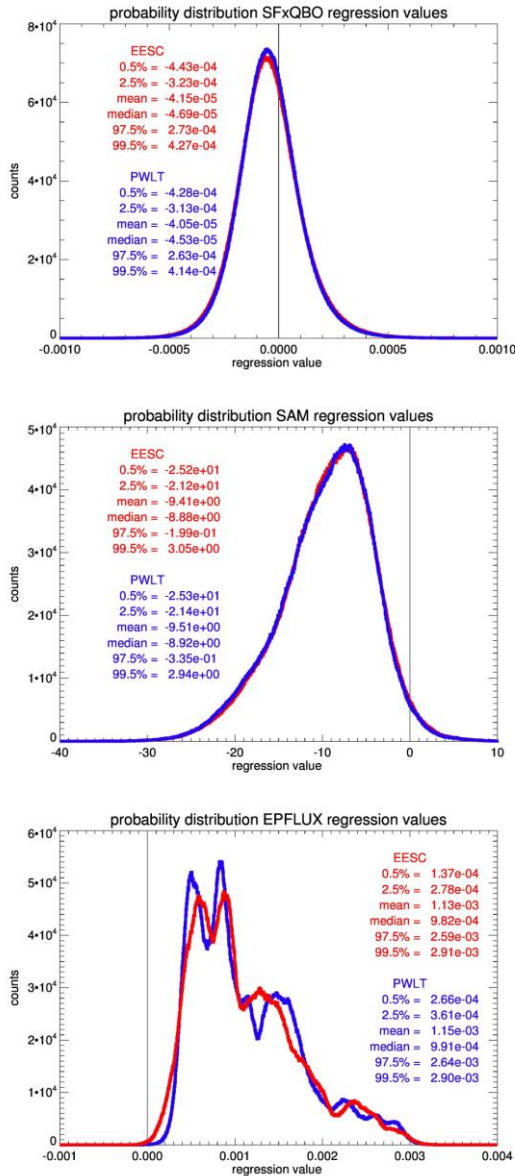
40

41 **Figure 5.** Probability distribution of regression model – ozone scenario correlations as  
 42 Figure 4, lower plot, for the PWLT and EESC regression model and sensitivity to the  
 43 different ozone scenarios and different EP flux scenarios, indicated by the different  
 44 colors. The blue and red outlines show the sum of all scenarios combined.



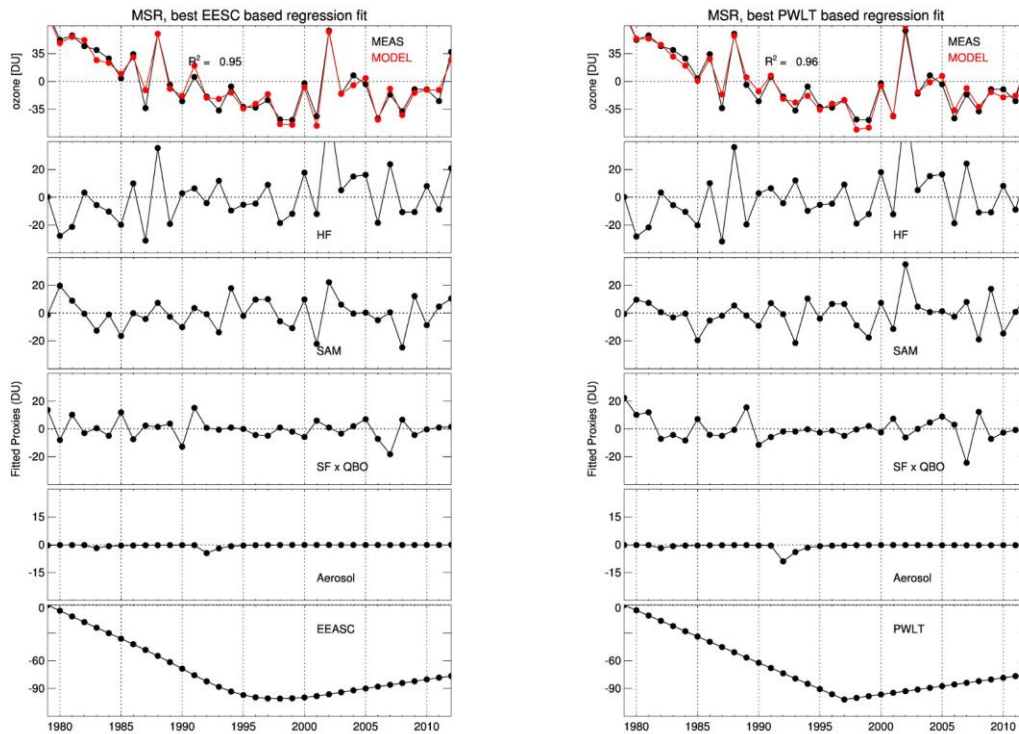
45

46 **Figure 6.** Upper panel: probability distribution of aerosol scenario regression coefficient  
 47 values of all PWLT regression results. Indicated in the figure are also the 0.5%-2.5%-  
 48 mean-median-97.5%-99.5% probability values of trends and correlations. Included are  
 49 also the distributions for the different stratospheric aerosol scenarios, indicated by the  
 50 different colors. Lower panel: probability distribution of the aerosol regression coefficient  
 51 values of the EESC regression model results. Included are also the distributions for the  
 52 three different EESC age of air scenarios, indicated by the different colors. The blue and  
 53 red outlines show the sum of all scenarios combined.



54

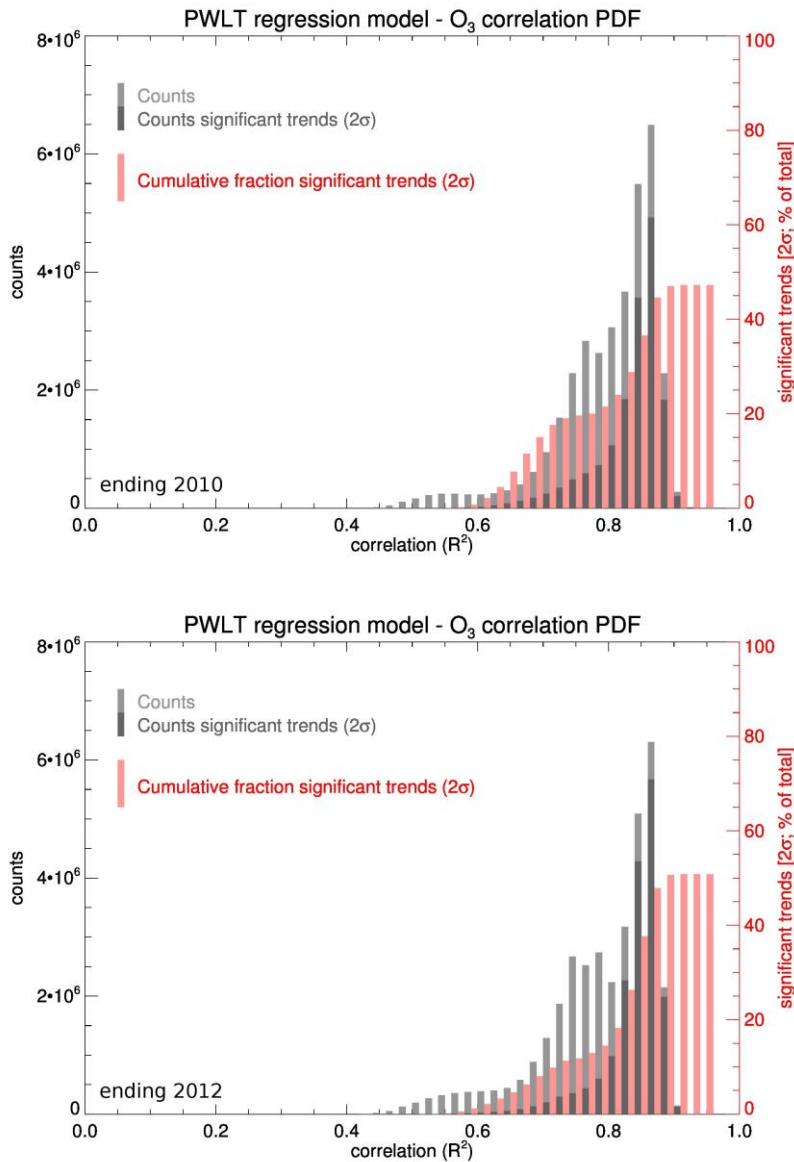
55 **Figure 7.** Panel A: probability distribution of the solar flux – QBO index regression  
 56 coefficient values of all EESC and PWLT regression model results. Panel B: probability  
 57 distribution of the SAM index regression coefficient values of all EESC and PWLT  
 58 regression model results. Panel C: probability distribution of the EP flux regression  
 59 coefficient values of all EESC and PWLT regression model results. Indicated in the  
 60 figure are also the 0.5%-2.5%-mean-median-97.5%-99.5% probability values of trends  
 61 and correlations.



63

64 **Figure 8.** Optimal regression model result for the EESC and PWLT and regressions  
 65 (upper panels, red line) as well as the corresponding ozone record scenario (upper panel,  
 66 black line). The ozone variations attributable to each are also shown. Ozone and ozone  
 67 anomalies are given in DU.





68

69 **Figure 9.** The probability distribution of regression model – ozone record scenario  
 70 correlations ( $R^2$ ) as shown in Figure 5 for the PWLT regressions and the cumulative  
 71 fraction of statistically significant ( $2\sigma$ ) ozone trends for each correlation interval (red,  
 72 right axis). The upper panel shows the distribution for the regressions ending in 2010, the  
 73 lower panel for the regressions ending in 2012. See also Table 7.

74

